Histidine Scanning Mutagenesis of Basic Residues of the S4 Segment of the *Shaker* K^+ Channel

Dorine M. Starace and Francisco Bezanilla

From the Department of Physiology and Department of Anesthesiology, University of California Los Angeles School of Medicine, Los Angeles, California 90095

ABSTRACT The voltage sensor of the *Shaker* potassium channel is comprised mostly of positively charged residues in the putative fourth transmembrane segment, S4 (Aggarwal, S.K., and R. MacKinnon. 1996. *Neuron.* 16: 1169–1177; Seoh, S.-A., D. Sigg, D.M. Papazian, and F. Bezanilla. 1996. *Neuron.* 16:1159–1167). Movement of the voltage sensor in response to a change in the membrane potential was examined indirectly by measuring how the accessibilities of residues in and around the sensor change with voltage. Each basic residue in the S4 segment was individually replaced with a histidine. If the histidine tag is part of the voltage sensor, then the gating charge displaced by the voltage sensor will include the histidine charge. Accessibility of the histidine to the bulk solution was therefore monitored as pH-dependent changes in the gating currents evoked by membrane potential pulses. Histidine scanning mutagenesis has several advantages over other similar techniques. Since histidine accessibility is detected by labeling with solution protons, very confined local environments can be resolved and labeling introduces minimal interference of voltage sensor motion. After histidine replacement of either residue K374 or R377, there was no titration of the gating currents with internal or external pH, indicating that these residues do not move in the transmembrane electric field or that they are always inaccessible. Histidine replacement of residues R365, R368, and R371, on the other hand, showed that each of these residues traverses entirely from internal exposure at hyperpolarized potentials to external exposure at depolarized potentials. This translocation enables the histidine to transport protons across the membrane in the presence of a pH gradient. In the case of 371H, depolarization drives the histidine to a position that forms a proton pore. Kinetic models of titrateable voltage sensors that account for proton transport and conduction are presented. Finally, the results presented here are incorporated into existing information to propose a model of voltage sensor movement and structure.

KEY WORDS: voltage sensor • potassium channel • proton transport • proton channel • gating current

INTRODUCTION

Voltage-gated ion channels are transmembrane proteins that couple the membrane potential to the opening and closing of an ion-selective pore (Hodgkin and Huxley, 1952). Voltage-dependent sodium, potassium, and calcium channels are fundamental to numerous physiological processes that rely on the rapid propagation of a stimulus or the maintenance of the membrane potential. In the nervous system, a well-known example, ionic current through voltage-gated Na^+ and K^+ channels generates the action potential and propagates it down the axon membrane. Pore opening in voltage-gated ion channels is initiated by the rearrangement of particular charged amino acids in response to a change of the electric potential across the membrane. The membrane potential–sensitive structure of the channel, which includes these charged amino acids, is known as the voltage sensor of the channel. The voltage sensor transduces a voltage change into conformational changes that culminate with the opening or closing of a molecular "gate" to the ion pore (for review see Bezanilla, 2000). Movement of the voltage sensor displaces charge, which can be measured as a transient current (called a gating current), that precedes the ionic current through the pore (Armstrong and Bezanilla, 1973; Keynes and Rojas, 1974). Electrophysiological studies of gating current behavior combined with site-directed mutagenesis have provided many molecular and kinetic details that underlie the operation of the voltage sensor. The recent combination of spectroscopy with traditional electrophysiological studies has begun to reveal some of the local structural changes that accompany voltage sensor movement.

The most abundant and detailed source of information about voltage-gated ion channels comes from studies of the *Shaker* K^+ channel. This channel is particularly amenable to studies of the voltage sensor since it expresses extremely well and its ionic conduction can be abolished by a pore mutation that does not significantly change the gating properties of the channel (Perozo et al., 1993). The *Shaker* K^+ channel is composed of four identical subunits, each containing six putative membrane spanning segments (S1–S6;

Address correspondence to Dr. Francisco Bezanilla, Department of Physiology, University of California, Los Angeles School of Medicine, 10833 Le Conte Avenue, Los Angeles, CA 90095. Fax: (310) 794-9612; E-mail: Fbezanil@ucla.edu

MacKinnon, 1991). The maximum gating charge displaced by the voltage sensor in each *Shaker* K^+ channel has been measured to be 12–13 charges (Schoppa et al., 1992; Aggarwal and MacKinnon, 1996; Noceti et al., 1996; Seoh et al., 1996). Most of the voltage-sensing residues are in the S4 segments of the channel (Aggarwal and MacKinnon, 1996; Seoh et al., 1996). Although every third amino acid in the S4 segment, from residue 362 to 377, is positively charged, only four of them, R362, R365, R368, and R371, clearly contribute charge to the gating current. Since the contribution of four full charges per subunit would result in the transfer of 16 rather than 12–13 charges across the transmembrane field, some or all of the voltage-sensing charges traverse only a fraction of the field. Clearly, an understanding of the molecular mechanisms underlying voltage sensitivity requires characterization of both the conformational changes that occur and the local electric field that determines charge movement.

Movement of the voltage sensor in response to a change in the membrane potential was examined indirectly by measuring how the accessibilities of residues in and around the sensor change with voltage In this paper, we use the technique of histidine scanning mutagenesis to probe residue accessibility. Five of the six basic residues in the S4 segment were individually replaced by a histidine to introduce a titrateable tag at various positions on or near the voltage sensor. Any changes in the solvent accessibility of the histidine that accompany transitions of the voltage sensor can be detected as pH-dependent changes in the gating currents. By simply manipulating the internal and external solution pH, and recording the subsequent gating currents evoked by membrane potential pulses, any changes in residue accessibility caused by voltage sensor transitions can be detected.

Histidine scanning mutagenesis has several advantages over other similar techniques such as cysteine scanning mutagenesis (Yang and Horn, 1995; Larsson et al., 1996; Yang et al., 1996; Yusaf et al., 1996; Baker et al., 1998). First, replacement of basic residues with histidine is less disruptive than other neutralizations because the native charge is maintained upon protonation. Second, labeling of the target histidine with protons is effectively instantaneous since the rate constants of protonation of a histidine residue (Eigen et al., 1960; Root and MacKinnon, 1994; Kasianowicz and Bezrukov, 1995) are much faster than the rate constants of gating transitions (Bezanilla et al., 1994). Finally, using protons to detect residue accessibility provides the maximum resolution achievable with tagging experiments since protons have access to spaces in the protein too confined for typical labeling reagents.

In this paper, we describe the histidine scanning method in detail, develop an extension of the theory presented previously (Starace et al., 1997), and present the results of scanning five of the basic residues of the *Shaker* K^+ channel S4 segment to probe local voltage-dependent accessibility changes. Upon histidine replacement, we found that charged residues at positions 365, 368, and 371 become consecutively exposed to inside or outside depending on the membrane potential. Consequently, in the presence of a transmembrane pH gradient, the histidine transports protons across the membrane with each stroke of the voltage sensor. This transfer of charge across the membrane confirms that residues 365, 368, and 371 are part of the voltage sensor, and that they contribute to the gating current. The results also provide evidence that, in both the resting and active states, these residues reside in aqueous crevices surrounded by anions of the bulk solution. Therefore, the large energy barrier to overcome in gating charge displacement would be the translocation of unpaired charges across the hydrophobic regions of the protein. In addition, we found that residues K374 and R377, when replaced by histidines, are not titrateable, indicating that they are not accessible or they do not contribute to the gating charge.

MATERIALS AND METHODS

Mutagenesis and Expression of Channels

The clone that was used as the background template for all mutagenesis and expression of *Shaker* K^+ channels contained the nonconducting (W434F; Perozo et al., 1993), fast inactivation–removed (IR, Δ6-46; Hoshi et al., 1990) *Shaker* H4 K^+ channel coding sequence (Schwarz et al., 1988). This clone, zH4IR[W434F], achieves very high expression levels in oocytes as a result of replacing the untranslated regions of the K^+ channel with those of *Xenopus* β-globin and inserting the Kozak consensus sequence, GCC-ACC (Kozak, 1991), immediately before the translational start site (Starace et al., 1997). All mutations of the zH4IR[W434F] clone were generated by PCR using the overlap extension method (Ho et al., 1989) and PCR-generated regions were sequenced. To express the channel, RNA was transcribed from the NotI-linearized DNA clone (New England Biolabs) with T7 RNA polymerase (mMessage mMachine™ in vitro transcription kit; Ambion) and 50 nl of 0.5–0.8 μg/μl cRNA was injected into each stage 5 *Xenopus* oocyte (Timpe et al., 1988). Injected oocytes were maintained at 18°C in an incubation solution of (in mM) 100 NaCl, 2 KCl, 1.8 $CaCl_2$, 1 $MgCl_2$, 5 HEPES, pH 7.3, 0.01 EDTA, and 0.5 DTT. The incubation solution was changed daily.

Electrophysiology

Channel currents were measured from oocytes 3–6 d after injection of channel cRNA. Currents were recorded at 20–23°C using the cut-open oocyte voltage clamp technique (Stefani and Bezanilla, 1998) or the patch-clamp technique (Hamill et al., 1981). Data was filtered at one fifth of the sampling frequency. Membrane potential test pulses to evoke currents were separated by at least 2 s.

Recording Solutions. The osmolarity of all recording solutions was 240–260 mOsm. NMDG-MS external solutions contained (in mM) 120 NMDG, 2 $CaCl_2$, and either 20 CHES (2-(*N*-cyclohexylamino)ethanesulfonic acid (for pH 9.2) or 20 HEPES (for all other pHs); all solutions were brought to the appropriate pH

with methanesulfonic acid (MS;[1] Fluka). NMDG-MS internal solutions were the same as the external solutions except that EGTA-NMDG replaced $CaCl_2$.

"High buffer" (HB) external solutions used Tris base and another acidic buffer (Sigma-Aldrich) as the main cation and anion, respectively; they were mixed to the desired pH and osmolarity. HB external solutions contained (in mM) 2 $CaCl_2$ along with (for pH 5.2) 21 Tris base and 246 Mes, or (for pH 6.3) 85 Tris and 152 Mes, or (for pH 7.4) 78 Tris and 178 HEPES, or (for pH 8.3) 146 Tris and 95 HEPES, or (for pH 9.2) 176 Tris and 44 CHES.

HB internal solutions used NMDG and an acidic buffer as the main cation and anion, respectively. They contained (in mM) 2 EGTA-NMDG along with (for pH 5) 17 NMDG and 236 Mes, or (for pH 7.4) 68 NMDG and 150 HEPES.

Patch-clamp Recordings. Currents were recorded from excised, inside-out macropatches using a P/4 protocol (subtracting holding potential = 30 or 40 mV) to digitally subtract linear capacity and leak components.

Cut-open Oocyte Voltage Clamp. The intracellular grounding electrode (V1) was filled with 2.7 M Na-MS and 10 mM NaCl. Currents were recorded unsubtracted after analogue compensation of linear membrane capacitance at 0–50 mV, where gating charge displacement has saturated. There was no subtraction or compensation of linear leak components while recording; they were subtracted off-line (see *Data Analysis*, *I-V Curves*).

For recordings of R368H and R371H channel currents, a second intracellular electrode was used to measure internal pH. Microelectrodes were pulled from acid-cleaned glass capillaries to tip diameters of ~1.5 μm, and then silanized by overnight exposure in a sealed container to dimethyloctylchlorosilane (Fluka) at 150°F. The tip of the electrode was filled with a liquid ion exchanger resin selective to H^+ (IE010; WPI, Inc.), and the remainder was filled with 3 M KCl. The H^+ electrode was mounted on the Vi headstage of the cut-open amplifier (Dagan) and balanced in the external solution with the grounding electrode (V1) right before impaling the oocyte with both electrodes. After impaling, intracellular pH was acquired as the potential difference between V1 and Vi. The response of the H^+ electrode was linear with pH, and the slope was determined after each oocyte by withdrawing both electrodes and recording V1-Vi in five different known pH solutions.

Data Analysis

Q-V Curves. Plots of the voltage dependence of gating charge displacement (Q) were obtained by integrating the transient component of pulse-evoked gating currents over the duration of the ON- or OFF-pulse. The steady-state value at the end of each pulse was used as the integration baseline. In some cases, the Q-V curves were fit to a sum of two Boltzmann distributions:

$$Q(V) = \frac{Q_1}{1+\exp[z_1(V_1-V)/25]} + \frac{Q_2}{1+\exp[z_2(V_2-V)/25]}.$$

Determination of C_g-V. To generate curves of the voltage dependence of gating capacitance ($C_g = dQ/dV$), the Q-V curve was fit to a sum of two Boltzmann distributions (shown above), and these fits were analytically differentiated with respect to voltage.

I-V Curves. The steady-state ON-gating current, an average over 1 ms starting at least 80 ms after the onset of the test pulse, was determined for each pulse potential in a pH_o group. This group of isochronal, steady-state current amplitudes was plotted as a function of test pulse potential. The component that increased linearly with voltage (leak) was fit to a straight line and subtracted from the isochronal current at each potential to produce the proton current amplitudes, I_H; the same linear leak value was also subtracted from the ON-gating currents. This correction method is valid since measurements of steady-state leak currents from uninjected oocytes and zH4IR[W434F] channels displayed conductances that were linear and pH-independent up to at least 10 mV (data not shown).

Fits of Proton I-V Curves to the Titrateable Voltage Sensor Models. Data sets of proton current I-V curves measured in several pH_os were simultaneously fit to model-derived expressions for the proton current. Analytical expressions for the proton current as a function of potential were derived from a titrateable voltage sensor model (see THEORY, second term of Eq. 1) or from a titrateable voltage sensor with a proton pore model (see THEORY, Eq. 6). The best fits of model to data sets were obtained using ScoP 3.5 simulation software (Simulation Resources, Inc.).

THEORY

A Titrateable Voltage Sensor Model

Gating currents can be modeled as charge-carrying transitions among states connected by voltage-dependent rate constants. A simple model of a voltage sensor with a protonatable residue (Fig. 1 A) was presented in detail in a previous publication (Starace et al., 1997). It provides a theoretical framework to understand the behavior of proton transport by a histidine-tagged voltage sensor, and enables us to estimate some physical parameters by fitting the data to the model. The voltage sensor can occupy states in **D** or **H**, in which its protonatable residue is exposed to the extracellular or intracellular solution, respectively. Transitions between **D** and **H** are driven by voltage-dependent rate constants, α_1, α_2, β_1, and β_2; hyperpolarization of the positively charged voltage sensor favors occupation of **H** states, and depolarization favors **D** states. The steepness of the voltage dependence of each the rate constants (α_n and β_n) is determined by the product of the valence of the state (z_n) and the fraction of the transmembrane electric field that the charge must traverse to hurdle the energy barrier of the state (δ_{α_n}):

$$\alpha_n(V) = \alpha_n(0)\exp[z_n\delta_{\alpha_n}FV/RT]$$

$$\beta_n(V) = \beta_n(0)\exp[-z_n(1-\delta_{\alpha_n})FV/RT].$$

On each side of the membrane, the voltage sensor can exist in a protonated state of valence, $z + z_1$, or an unprotonated state of valence, z. The equilibrium between the two states is dependent on the pK_a of the titrateable residue and the pH of the surrounding solvent. We assume that this equilibrium is reached infinitely fast since, on average, voltage sensor transitions occur at a limiting rate ~10 times slower than proton dissociation rates (Eigen et al., 1960; Root and MacKinnon, 1994; Kasianowicz and Bezrukov, 1995). Then, states **D** and **H** each consist of a mixture of states in fast equilibrium; f_i, the fraction of internally exposed voltage sensors in the protonated state can be expressed as

$$f_i = \frac{1}{1+\exp[2.3(pH_i-pK_i)]}$$

and f_o, the fraction of externally exposed, protonated voltage sensors can be expressed as

$$f_o = \frac{1}{1+\exp[2.3(pH_o-pK_o)]}.$$

The transitions of the voltage sensor between **D** and **H** states move charge ze_o or $(z + z_1)e_o$ across the transmembrane electric field, and thereby generate a gating current. For N subunits, the ON-gating current, i_g, produced upon depolarization from an ex-

[1]*Abbreviations used in this paper:* HB, high buffer; MS, methanesulfonic acid; pH_i, internal pH; pH_o, external pH.

tremely hyperpolarized initial state to various test potentials, *V*, contains a transient, exponentially decaying component and a steady component given by

$$i_g(t,V) = \frac{N e_0 \alpha'}{\alpha' + \beta'}[z(\alpha' + \beta') + z_1(\alpha_1 f_i + \beta_1 f_o)]\, e^{-(\alpha' + \beta')t} + \frac{N e_0 z_1 (\alpha_1 \beta' f_i - \alpha' \beta_1 f_o)}{\alpha' + \beta'}, \quad (1)$$

where α' and β' are composite forward and backward rate constants (Starace et al., 1997). The second, steady component is the proton transport current carried by the titrateable residue. The transport current has a bell-shaped or biphasic voltage dependence since it goes to zero at very hyperpolarized or depolarized potentials as either the forward or backward rate constants approach zero.

In the model outlined above, the internal and external pK_as of the titrateable residue are constant values. However, it is possible that the titrateable residue is situated in a confined aqueous environment into which the transmembrane electric field extends. The presence of a field will alter the local pH around the titrateable residue by affecting the access of protons to their binding site. To accommodate this possibility, a term describing a proton in an electric field can be added to pK_o and pK_i to convey apparent voltage dependence:

$$pK_o(V) = pK_o(0) - [\delta_o FV/(2.3RT)] \quad \text{and} \quad pK_i(V) = pK_i(0) + [\delta_i FV/(2.3RT)], \quad (2)$$

where δ is the fraction of the transmembrane electric field sensed, F is the Faraday constant, *R* is the gas constant and *T* is the temperature.

At $V = E_{H+}$, the Nernst equilibrium potential, there can be no net proton flow across the membrane:

$$\alpha_1 \beta_2 K_o[H_i] = \alpha_2 \beta_1 K_i[H_o].$$

The above requirement of microscopic reversibility at equilibrium imposes the following constraint on the relationship between the rate constants:

$$\beta_2(0) = \frac{\alpha_2(0)\beta_1(0)}{\alpha_1(0)} \times \exp\{2.3[pK_o(0) - pK_i(0) + (pH_i - pH_o)(1 - z_1 - \delta_i - \delta_o)]\}. \quad (3)$$

Titrateable Voltage Sensor Model with a Proton Pore

Fig. 1 B shows an extension of the titrateable voltage sensor model in which both proton transport and conduction can take place. The extended model predicts gating current behavior when depolarization drives the titrateable residue to a position accessible from both the internal and external solutions simultaneously. This creates a proton pore gated open by depolarization of a titrateable voltage sensor.

The proton pore was modeled by allowing deprotonation in the EH state or protonation in the E state from protons in either the internal (H_i) or external (H_o) solution (Fig. 1 B). Therefore, the fast equilibrium between EH and E states is dependent on both (1) pH_i and pK_{iP}, the internal pK_a of the titrateable residue occupying **D** states, and (2) pH_o and pK_o, the external pK_a of the titrateable residue occupying **D** states. To accommodate the possibility that the proton binding site of the pore is located in the transmembrane field, pK_o and pK_{iP} also have voltage-dependent terms with coefficients δ_o and δ_{iP}, respectively (as in Eq. 2).

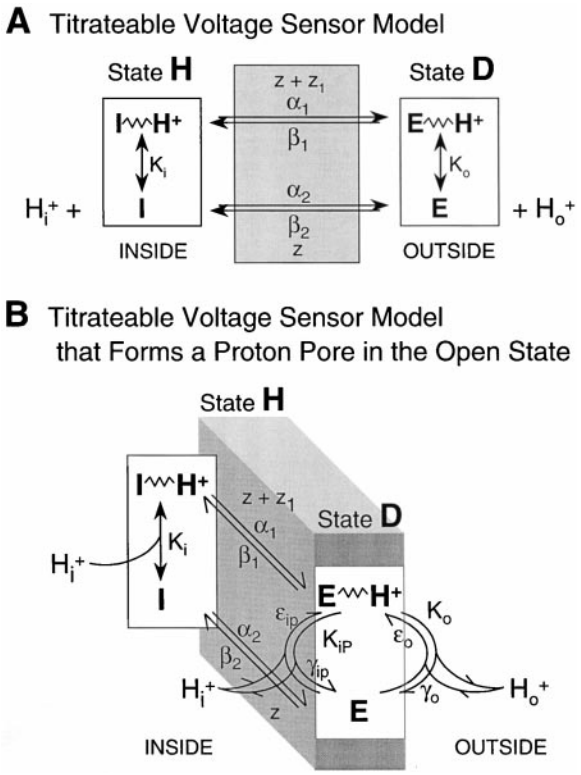

FIGURE 1. Titrateable voltage sensor models. (A) Gating currents were modeled as transitions between **H** and **D** connected by voltage-dependent rate constants α and β. The charge carried by the titrateable voltage sensor in each transition between **H** and **D** is either z or $z + z_1$, as determined by the equilibrium dissociation constant, pK (K_i or K_o), of the titrateable group and the surrounding pH (H_i^+ or H_o^+ if the titrateable group gets exposed to the internal or external solution, respectively). Since the S4 segment, which contains most of the voltage sensing residues, is positively charged, depolarization of the membrane (gray box) moves the voltage sensor from the inside of the membrane towards the outside, thereby moving charge z or $z + z_1$, in the transition. (B) The titrateable voltage sensor model shown in A was extended to incorporate the formation of a one-ion proton pore at depolarized potentials. In the **D** states, the titrateable residue has access to both the internal and external solutions simultaneously, and this creates a proton pathway through the membrane. Proton binding in the **D** states from the external solution depends on the dissociation constant, pK_o ($K_o = \gamma_o/\varepsilon_o$) and the external pH ($H_o$); binding from the internal solution depends on pK_{iP} ($K_{iP} = \gamma_{ip}/\varepsilon_{ip}$) and pH_i.

At the Nernst equilibrium potential, there can be no net proton flow across the membrane:

$$\alpha_1 \beta_2 K_o[H_i] = \alpha_2 \beta_1 K_i[H_o]$$
$$K_o[H_i] = K_{iP}[H_o].$$

The first of these requirements of microscopic reversibility at equilibrium imposes the constraint shown in Eq. 3, and the second requirement imposes the following constraint on the relationship between the pore parameters:

$$pK_{iP}(0) = pK_o(0) + (pH_i - pH_o)(1 - \delta_o - \delta_{iP}).$$

The expression for the ON-gating current given in Eq. 1 for the titrateable voltage sensor model can be used for the ex-

tended pore model after a couple of modifications. First, the expression for f_o, the fraction of externally exposed protonated voltage sensors, must be altered to accommodate the additional pathways in the **D** states. Second, a term describing proton conduction in the **D** states must be added to the ON-gating current. With the external pore states assumed to be fast equilibrium, the steady-state expression for f_o becomes

$$f_o = \frac{[EH]}{[EH]+[E]} = \frac{H_i\varepsilon_{ip} + H_o\varepsilon_o}{\varepsilon_o(H_o + K_o) + \varepsilon_{ip}(H_i + K_{iP})}$$
$$= \frac{1 + (\varepsilon_{ip}/\varepsilon_o)e^{2.3(pH_o - pH_i)}}{1 + (\varepsilon_{ip}/\varepsilon_o)e^{2.3(pH_o - pH_i)} + e^{2.3pH_o}[e^{-2.3pK_o} + (\varepsilon_{ip}/\varepsilon_o)e^{-2.3pK_{iP}}]}. \quad (4)$$

The expression for the net proton current, I_P, through the one-ion binding pore (Hille, 1992) formed in the **D** states in steady state is given by

$$I_P = Nz_He_0\mathbf{D}[\gamma_o f_o - \varepsilon_o H_o(1 - f_o)],$$

where z_H is the proton valence and **D** is the probability of occupying state **D** (Fig. 1 B; derived in Starace et al., 1997). After substitution of **D**, the steady-state component of the proton pore current is

$$I_P = \frac{Nz_He_0\alpha'\varepsilon_o e^{-2.3pH_o}}{\alpha' + \beta'}[f_o(1 + e^{-2.3(pK_o - pH_o)}) - 1]. \quad (5)$$

Finally, the steady-state component of the ON-gating current, I_H, predicted by the model of a titrateable voltage sensor with a pore, is the sum of the proton pore current, I_P (Eq. 5) and the proton transport current, I_T, (Eq. 1) using the expression for f_o given in Eq. 4:

$$I_H = I_T + I_P = \frac{Nz_1e_0(\alpha_1\beta' f_i - \alpha'\beta_1 f_o)}{\alpha' + \beta'} + \frac{Nz_He_0\alpha'\varepsilon_o e^{-2.3pH_o}}{\alpha' + \beta'}[f_o(1 + e^{-2.3(pK_o - pH_o)}) - 1]. \quad (6)$$

RESULTS

To examine residue accessibility changes that accompany charge displacement during *Shaker* K^+ channel gating, we individually replaced each charged residue in the S4 segment with histidine. Each histidine replacement was made in a nonconducting (W434F; Perozo et al., 1993), nonfast-inactivating (IR, Δ6-46; Hoshi et al., 1990) version of the channel so that the steady-state properties of gating could be examined. The histidine-replaced channels will be referred to simply by the additional mutations made in this nonconducting, noninactivating background. If displacement of the voltage sensor causes exposure of the histidine tag to the bulk solution, its charge can be titrated with the pH of the surrounding solution. In each histidine mutant, the charge displaced by the voltage sensor was determined by measuring the gating currents from expressed channels. Under membrane voltage clamp, an ON-gating current was evoked by the onset of various test pulses from an extremely hyperpolarized membrane potential (−90 to −130 mV) and an OFF-gating current by the return to hyperpolarized potential. The elicited gating currents are transient, capacitive currents since they result from the rearrangement of permanent charges in the channel in response to a change in the transmembrane potential. Gating charge displacement (Q) was determined by integrating the gating currents.

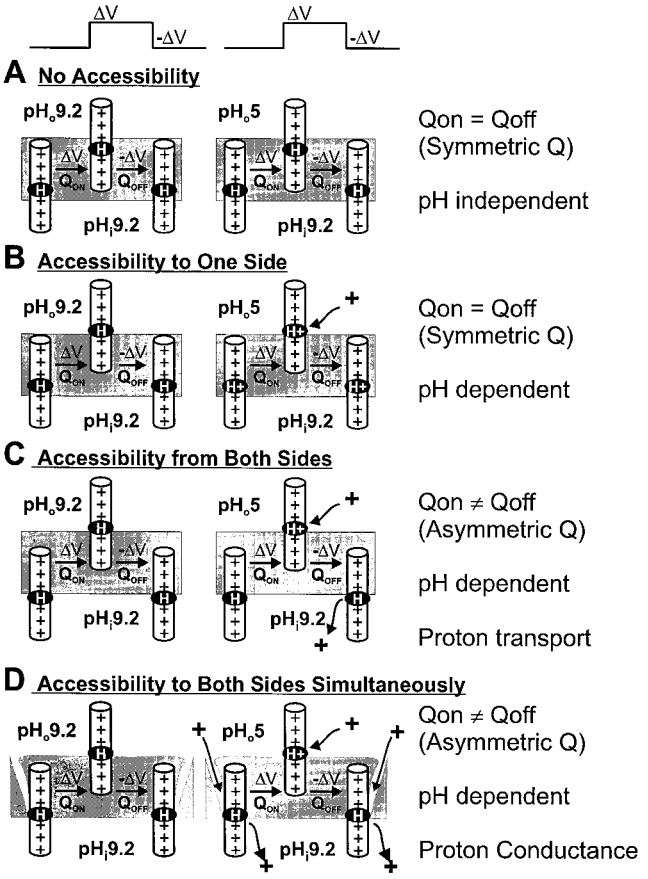

FIGURE 2. Histidine scanning mutagenesis. The various experimental outcomes of histidine scanning mutagenesis (summarized in text on the right) depend on the accessibility of the histidine (H, unprotonated; H^+, protonated) to solution protons during gating. Histidine accessibility during gating is monitored as pH-dependent changes in the gating charge displacement (Q) evoked by membrane potential pulses (shown at top). A depolarizing pulse (ΔV) moves the positively charged voltage sensor (represented as a cylinder) from the inside of the membrane (gray box) towards the outside, thereby displacing gating charge Q_{on}. Repolarization (−ΔV) returns the gating charge Q_{off}. If the histidine is part of the voltage sensor, modulation of Q_{on} by the internal pH (pH_i) indicates internal exposure and modulation of Q_{off} by the external pH (pH_o) indicates external exposure. The relationship between Q_{on} and Q_{off} is shown schematically in pH_o/pH_i 9.2/9.2 (left) and in pH_o/pH_i 5/9.2 (right) for four different histidine exposure possibilities.

The various experimental outcomes of using histidine scanning mutagenesis to tag the voltage sensor are shown schematically in Fig. 2. If the inserted histidine is

not a voltage-sensing residue that moves relative to the transmembrane electric field, its charge will not be part of the gating charge measurement and no conclusions can be made. The first case we consider in Fig. 2 A is that the histidine is not accessible at all during gating. A depolarizing pulse (ΔV) moves the histidine, along with the positively charged S4 segment (represented as a cylinder), from the inside of the membrane towards the outside, thereby displacing gating charge, Q_{on}. Repolarization ($-\Delta V$) returns gating charge Q_{off}. If always inaccessible to the surrounding solution, the histidine charge will be unaffected by the solution pH; consequently, Q_{on} and Q_{off} will be equal and pH-independent. Of course, a totally inaccessible histidine that contributes its charge to gating is indistinguishable from a histidine that does not move in the electric field.

The second case (Fig. 2 B) is one in which, during gating, the histidine moves from a buried position to a position that is exposed to one side of the membrane. In this case, the histidine charge will depend on the pH of the solution on the side where histidine gets exposed. For instance, a histidine that surfaces to the external solution with movement of the voltage sensor will equilibrate with the pH of the external solution. Then, in low external pH (Fig. 2 B, right), the voltage sensor will move more charge than in high external pH (Fig. 2 B, left); Q_{on} and Q_{off} will be equally modulated by the pH on the side of histidine exposure, since the histidine charge determined on exposure will not change once in the buried position. Therefore, in the case that voltage sensor displacement is accompanied by exposure of the histidine tag to one side of the membrane, gating charge displacement will be pH-dependent and symmetric ($Q_{on} = Q_{off}$).

A third possible outcome of histidine scanning mutagenesis is that voltage sensor displacement drives histidine exposure from one side of the membrane to the other (Fig. 2 C). In this case, when a pH gradient is applied across the membrane, the histidine will bind a proton once exposed to the low pH side and release it once exposed to the high pH side (Fig. 2 C, right). The histidine translocation thereby generates a proton transport current down the proton electrochemical gradient. Since the histidine traverse is coupled to voltage sensor movement, the proton transport current will have a voltage dependence coupled to the voltage dependence of gating charge displacement (Q). Charge displacement by the voltage sensor saturates at a minimum or maximum value at very hyperpolarized or depolarized potentials, respectively. At the potential of half-maximal charge displacement ($V_{1/2}$, the midpoint of the Q-V curve), it is equally probable that the voltage sensor occupies its hyperpolarized-favored state or its depolarized-favored state, so that the frequency of transitions between the two states is greatest. Since the histidine oscillates between internal and external exposure with each of these voltage sensor transitions, it will generate a sustained proton transport current that peaks near $V_{1/2}$ if the proton electrochemical driving force does not change direction (if the Nernst proton equilibrium potential E_{H+} is not near $V_{1/2}$). If E_{H+} falls near $V_{1/2}$, then the voltage sensor–coupled transport current will exhibit biphasic behavior, reversing at E_{H+}. In either case, the size of the proton current will decrease with the frequency of voltage sensor transitions and approach zero at very hyperpolarized or depolarized potentials as the transitions become more infrequent and the voltage sensor remains in one state most of the time. Thus, it is expected that the voltage dependence of proton transport by the histidine will be bell-shaped or biphasic, and will correspond to the voltage dependence of the capacitance of charge displacement (dQ/dV) weighted by the proton electrochemical gradient. The correspondence will not be exact since proton transport tracks one residue in the voltage sensor, whereas charge displacement tracks the entire voltage sensor.

Another consequence of the case in which the histidine tag traverses the membrane during gating is asymmetric charge displacement ($Q_{on} \neq Q_{off}$) in a pH gradient (Fig. 2 C). The histidine will more likely bind a proton on the lower pH side and release it on the high pH side. Therefore, the charge displaced by the voltage sensor when the histidine is exposed to the high pH side will be less than the charge that returns after histidine equilibration on the low pH side. Histidine exposure in the resting, hyperpolarized state is indicated by Q_{on} since it is the charge displaced from the resting state. In general, titration of Q_{on} by the internal pH (pH_i) indicates internal exposure when hyperpolarized, whereas titration of Q_{on} by the external pH (pH_o) indicates external exposure. Likewise, histidine exposure in the active, depolarized state is indicated by Q_{off} since it is the charge returning from the pulsed, depolarized states; titration of Q_{off} by pH_i indicates internal exposure when depolarized, whereas titration of Q_{off} by pH_o indicates external exposure.

A fourth possible outcome of histidine scanning mutagenesis is that, in one of the states occupied by the voltage sensor, the histidine spans the gap between the internal and external solution, creating a proton pore or channel (Fig. 2 D). The voltage dependence of the proton current through this pore would not be bell-shaped as expected for the transport case discussed above. Rather, the pore would be gated open by the voltage sensor at the potential where the probability that the histidine makes the bridge is maximal. Thereafter, the proton current amplitude through the histidine channel would continuously increase with voltage and pH gradient.

Nontitrateable Residues

R377H Channel. The arginine at position 377 is presumably the most internally facing charged residue in the S4 segment. Its contribution to voltage sensing is unknown since mutations that alter this charge have not produced functional channels (Aggarwal and MacKinnon, 1996). When R377 was replaced by a histidine, however, the channel expressed and was functional. Fig. 3 A shows R377H channel gating currents in response to various test pulses recorded from an inside-out macropatch in symmetrical pH 7.4 solutions. They are very similar to those of a wild-type channel. The voltage dependence of gating charge displacement (Q-V curve) for the ON- and OFF-gating currents, shown side by side in Fig. 3 C (triangles), fit to a sum of two Boltzmann processes with a midpoint of maximal Q displacement around −35 mV. It is clear that, as expected, at potentials that saturate charge displacement to its maximum value, the maximum Q displaced in the ON-gating current (0.9 pC) is equal to the Q returning in the OFF-gating current. In fact, Q_{on} and Q_{off} are approximately symmetric at each potential applied (Fig. 3 C, inset).

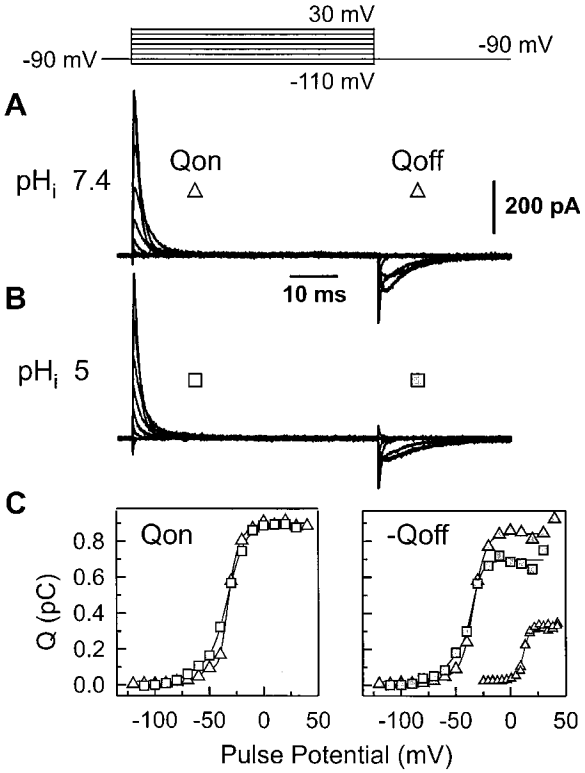

FIGURE 3. Gating charge displacement in the R377H channel is unaffected by internal protons. (A) Gating current records from the R377H channel measured from an inside-out macropatch in symmetric NMDG-MS pH 7.4 solutions. The superimposed currents are in response to various test pulses from a holding potential of −90 mV, also shown superimposed at the top. Onset of the test pulse stimulates an ON-gating current (Q_{on}), and repolarization of the membrane causes the returning OFF-gating current (Q_{off}). (B) The same sequence of superimposed gating current records from the same macropatch after exchange of the pH 7.4 internal solution (pH$_i$ 7.4) with a pH$_i$ 5 internal solution. (C) ON- and OFF- gating currents were each integrated over time and plotted as a function of pulse potential to obtain the voltage dependence of steady-state charge displacement (Q-V curves). Q-V curves are shown for the ON- (left panel, open symbols) and OFF-gating currents (right panel, closed symbols) displayed in A (pH$_i$ 7.4, triangles) and B (pH$_i$ 5, squares). The ON and OFF Q-V curves for the gating currents measured in symmetric pH 7.4 solutions are plotted on the same graph in the inset of the right panel. Each Q-V curve was fit to a sum of two Boltzmann distributions (lines). (Experiment D03238a)

When the internal pH (pH$_i$) was changed to pH 5, there was no significant change in the gating currents (Fig. 3 B). Fig. 3 C compares the Q-V relationships of the ON- and OFF-gating currents recorded in pH$_i$ 5 (squares) and pH$_i$ 7.4 (triangles). If the histidine at 377 were part of the voltage sensor and exposed to the internal solution in the closed, hyperpolarized state, then the charge it would contribute to the ON-gating current would increase with decreasing pH$_i$ as the population of protonated histidines grew. However, there was no increase in maximum Q_{on} with an increase of internal proton concentration from pH$_i$ 7.4 to pH$_i$ 5 (Fig. 3 C, Q_{on}). The small increase in Q_{on} at around −50 mV is not due to internal exposure, but to a difference in the kinetics between pH$_i$ 5 and pH$_i$ 7.4 that can be seen qualitatively in comparing the gating current records (Fig. 3, A and B).

If the histidines were internally exposed in any of the states induced by the test pulse, then the charge returning in the OFF-gating current upon repolarization would increase with decreasing pH$_i$. However, there was no such increase in Q_{off} when pH$_i$ was changed from 7.4 to 5. In fact, the maximum Q_{off} decreased a bit (Fig. 3 C, $-Q_{off}$), a commonly observed idiosyncrasy in excised patches caused by a slowing down of the OFF-gating currents upon excision, seen in Fig. 3 B (Sigg et al., 1994). Since pH$_i$ does not affect the gating charge displaced in the R377H channel, no matter what state the channel is clamped to, the histidine at position 377 must be always inaccessible from the internal solution or it is not part of the voltage sensor.

The effects of external pH (pH$_o$) changes on R377H channel gating currents were examined in the cut-open oocyte voltage clamp configuration. Holding the R377H channel at −90 mV in pH 7.4 internal solution, a range of pulse-induced gating currents was recorded from the same oocyte in pH$_o$ 9.2 (Fig. 4 A) and pH$_o$ 5 (Fig. 4 B). Comparison of R377H channel gating currents measured with the cut-open voltage clamp (Fig. 4, A and B) and those measured from an excised macropatch (Fig. 3, A and B) highlights the slowing kinetics of the OFF-gating currents upon excision of a patch.

When pH$_o$ was changed from 9.2 to 5, there were no significant changes in the R377H channel gating cur-

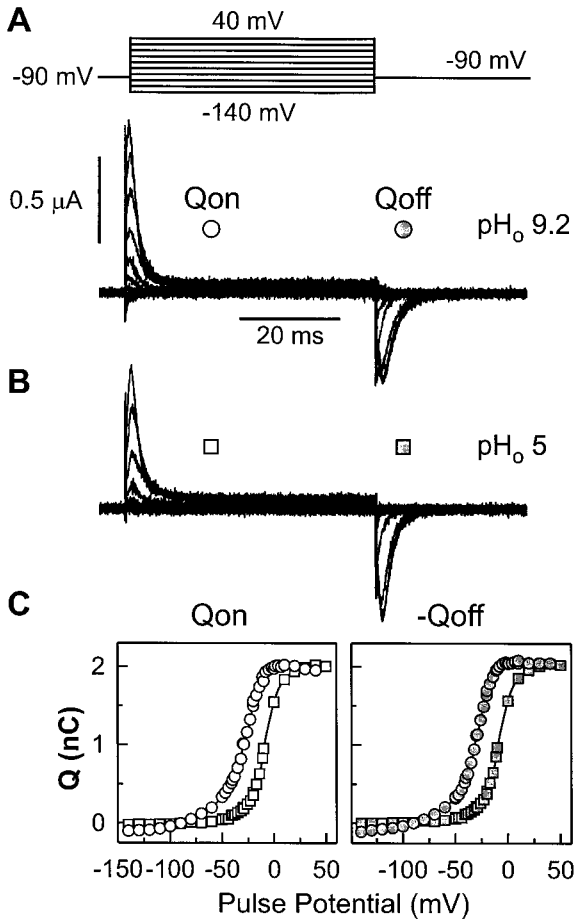

FIGURE 4. Gating charge displacement in the R377H channel is unaffected by external protons. (A) Gating current records from the R377H channel measured with the cut-open oocyte voltage clamp in symmetric NMDG-MS solutions, pH 7.4 in the inside and pH 9.2 in the outside (pH$_o$). The superimposed currents are in response to various test pulses from a holding potential of −90 mV, also shown superimposed at the top. (B) The same sequence of superimposed gating current records from the same oocyte in pH$_o$ 5 external solution. (C) The voltage dependence of gating charge displacement (Q-V curves) for the ON- (left panel, open symbols) and OFF-gating currents (right panel, closed symbols) displayed in A (pH$_o$ 9.2, circles) and B (pH$_o$ 5, squares). (Experiment D11017h)

rents (Fig. 4 B). However, the voltage dependence of charge displacement in pH$_o$ 5 was shifted by about +20 mV (Fig. 4 C, squares) relative to the Q-V curve in pH$_o$ 9.2 (Fig. 4 C, circles). This shift of the Q-V curve to more depolarized potentials with a decrease in pH$_o$ arises from a screening of fixed charges on the membrane surface by external protons (Hille, 1992), a phenomenon also observed in control channels without a histidine replacement (data not shown). Aside from the voltage shift, which is unrelated to the histidine charge, there is no change in the Q-V curve induced by a change of pH$_o$. The inefficacy of both internal and external protons to titrate R377H gating currents demonstrates that either the histidine at position 377 is buried in every conformation occupied from minimum to maximum gating charge displacement, or that it does not move in the electric field.

K374H Channel. The fifth charged residue in S4 is a lysine at position 374, approximately one helical turn from R377, if S4 has an α-helical structure. Although the charge contributed by K374 to the gating current has been measured directly, the role of K374 in voltage sensing is still ambiguous (Aggarwal and MacKinnon, 1996; Seoh et al., 1996). Most mutations that neutralize the amino acid at 374 hinder functional expression of the channel. Replacement of the lysine at position 374 with a histidine did not dramatically alter the expression or voltage sensitivity of the channel (Fig. 5 A). A series of pulse-induced gating currents from the K374H channel that encompasses the full range of charge displacement is shown in Fig. 5 A. The currents were recorded from an excised, inside-out macropatch in pH$_o$ 9.2 and pH$_i$ 7.4 solutions. The Q-V curves derived from the ON- and OFF-gating currents are shown superimposed in Fig. 5 C (triangles). Although there is a pH gradient across the membrane, Q_{on} and Q_{off} are symmetric at each potential. Therefore, the histidine at 374 is either not accessible at all during gating or it passes through a state exposed to one side of the membrane exclusively (Fig. 2).

To determine whether the histidine at 374 inhabits any internally exposed states, the internal solution was perfused with pH$_i$ 5 solution, and gating currents in response to 0- or 20-mV test pulses were intermittently recorded during the perfusion (Fig. 5 B). We expected Q measured in pH$_i$ 5 to be saturated at its maximal value at 0 mV since it is saturated in pH$_i$ 7.4. Moreover, if there were any shift at all in the pH$_i$ 5 Q-V curve due to surface charge screening, it would be in the negative direction. Comparison of Q measured before and during pH$_i$ 5 perfusion (Fig. 5 D) indicates that neither Q_{on} nor Q_{off} are significantly altered by a reduction of pH$_i$. Clearly, there is no increase of maximal gating charge displacement due to increased protonation of the histidine. In Fig. 5 C, the average Q_{on} and Q_{off} elicited by 0- and 20-mV test pulses during pH$_i$ 5 perfusion (squares) are displayed with the entire Q-V curve measured in pH$_i$ 7.4 (triangles). In pH$_i$ 5, Q is the same at 0 and 20 mV, confirming that the charge displacement measured in pH$_i$ 5 was indeed maximal. Since there was no change in the total gating charge with a change of pH$_i$, the histidine at position 374 is internally inaccessible throughout gating or it does not contribute to the charge displaced during gating.

To determine whether the histidine at position 374 gets exposed to the external side during gating, the effect of pH$_o$ on K374H channel gating currents was examined with the cut-open oocyte voltage clamp. A series of test pulse-induced gating currents encompassing the

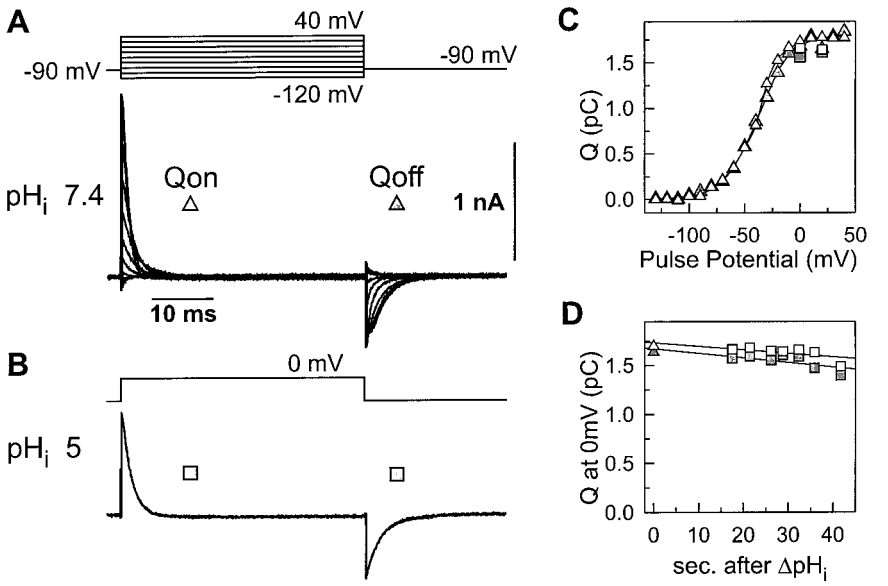

FIGURE 5. Gating charge displacement in the K374H channel is unaffected by internal protons. (A) Gating current records from the K374H channel measured from an excised inside-out macropatch in symmetric NMDG-MS solutions, pH 9.2 in the outside and pH 7.4 in the inside (pH$_i$). The superimposed currents are in response to various test pulses from a holding potential of −90 mV, shown superimposed at the top. (B) Gating current in response to a 0 mV test pulse from the same macropatch during perfusion of pH$_i$ 5 internal solution. (C) Q-V curves for the ON- (open symbols) and OFF-gating currents (closed symbols) displayed in A (pH$_i$ 7.4, triangles). Each Q-V curve was fit to a sum of two Boltzmann distributions (lines). The internal side was perfused with pH$_i$ 5 solution, and test pulses to 0 mV were intermittently applied 20 s later to measure the saturating charge displacement. A test pulse to 20 mV was also applied once to confirm saturation of charge displacement. The average of the charge displaced in the ON- and OFF- gating currents from seven of these 0-mV test pulses and the 20 mV pulse during pH$_i$ 5 perfusion are shown (squares). (D) Q_{on} (open symbols) and Q_{off} (closed symbols) in response to 0 mV test pulses measured in pH$_i$ 7.4 (triangles) and during internal pH$_i$ 5 perfusion (squares). The lines through the data are linear regressions. (Experiment D11077b)

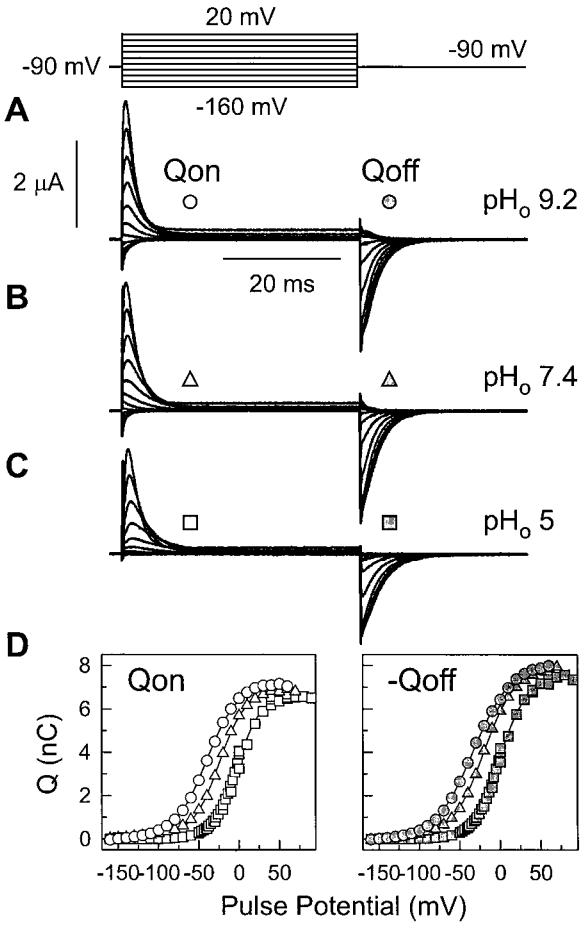

full range of charge displacement was recorded in three different pH$_o$s from the same oocyte (Fig. 6, A–C). An increase of external proton concentration from pH$_o$ 9.2 to 5 did not increase maximum Q_{on} or Q_{off} (Fig. 6 D). The only difference in the Q-V curves caused by a change of pH$_o$ was a shift along the voltage axis by about +8 mV per 100-fold increase in proton concentration. As described above, this external pH effect is not related to the charge or presence of the histidine, but is caused by the screening of surface charges by protons.

Since changes in pH$_o$ and pH$_i$ have no affect on the total gating charge displacement in the K374H channel, the histidine at position 374 is buried in all of the conformations occupied during gating. Alternatively, H374 is not part of the voltage sensor and its charge, whether titrated by solution protons or not, does not move in the transmembrane electric field.

FIGURE 6. Gating charge displacement in the K374H channel is unaffected by external protons. (A) Gating current records from the K374H channel measured in the cut-open oocyte configuration in symmetric NMDG-MS pH 9.2 solutions (pH$_i$ 9.2 and pH$_o$ 9.2). The superimposed currents are in response to various test pulses from a holding potential of −90 mV, also shown superimposed at the top. (B) The same sequence of superimposed gating current records from the same oocyte in pH$_o$ 7.4 external solution. (C) The same sequence of superimposed gating current records from the same oocyte in pH$_o$ 5 external solution. (D) Q-V curves for the ON- (left panel, open symbols) and OFF-gating currents (right panel, closed symbols) displayed in A (pH$_o$ 9.2, circles), B (pH$_o$ 7.4, triangles), and C (pH$_o$ 5, squares). (Experiment D06088a)

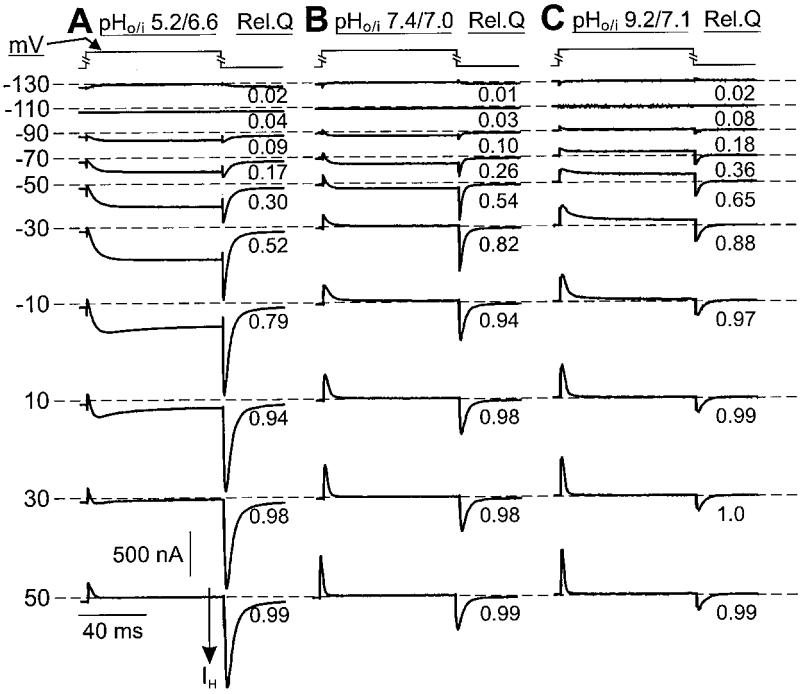

FIGURE 7. Gating currents of the R368H channel displace titrateable charge and transport protons. Using the cut-open oocyte voltage clamp, R368H channel gating currents were recorded in internal HB solution, pH 7.4, and various external HB solutions (A, pH_o 5.2; B, pH_o 7.4; C, pH_o 9.2). The intracellular pH (pH_i) was measured with a H^+-sensitive electrode. All gating currents were recorded from the same membrane area. The gating currents in each pH_o group were elicited by a family of test pulses (in millivolts) from a pre- and postpotential pulse of −110 mV (represented at the top of each group). The test pulse value corresponding to each current is shown on the left. The normalized charge displacement in each gating current (Rel. Q, shown to the right of each trace) was obtained by integrating the OFF-gating currents (Fig. 9 B) and normalizing to the maximum value of each pH_o group. Linear leak current was subtracted from each current trace off-line as described in MATERIALS AND METHODS (*Data Analysis of I-V Curves*). (Experiment D11200a)

Residues that Traverse the Membrane during Gating

The central three basic residues of the S4 segment, R365, R368, and R371, contribute charge to the gating current and, therefore, form part of the voltage sensor of the channel (Aggarwal and MacKinnon, 1996; Seoh et al., 1996). Histidine replacement studies of R365 and R368 have shown that, in each case, the histidine traverses from internal to external exposure during gating (Starace et al., 1997). This translocation enables the histidine, driven by voltage sensor transitions, to transport protons across the membrane in the direction of the proton electrochemical gradient. A simple kinetic model of a titrateable voltage sensor (Starace et al., 1997) fits quite well to the proton transport currents, and can be used to estimate various physical parameters including transport rates and pK_as.

R368H Channel. Fig. 7 shows three series of pulse-induced gating currents from the R368H channel, each encompassing the full range of charge displacement in a different pH gradient. The pH gradients were imposed by varying the external pH (pH_o) while leaving the internal solution constant. Since control of pH_i is not precise in cut-open oocyte voltage clamp configuration, pH_i was measured with a proton-selective microelectrode. The gating currents of the R368H channel look very different from the gating currents shown previously. The ON-gating current is a superposition of the typical transient charge displacement that decays to zero and a steady proton current transported by the histidine. In the presence of an inward proton gradient that establishes a very depolarized proton equilibrium potential, E_{H+} (Fig. 7 A), an inward current developed during ON-gating, increased as the membrane was increasingly depolarized, peaked at around −30 mV, and then decreased and became zero at very depolarized potentials. The size of the inward current was reduced (Fig. 7 B) when the proton gradient was reduced, and thereby decreased the proton electrochemical driving force in the voltage region of charge displacement. Reversal of the pH gradient to establish a very hyperpolarized E_{H+} resulted in an outward steady current also with a bell-shaped voltage dependence (Fig. 7 C). The appearance of a steady current driven by the proton electrochemical gradient only in the voltage region of frequent voltage sensor transitions indicates that it is a current of protons transported across the membrane by the histidine at position 368.

It is curious that at depolarized membrane potentials (greater than or equal to −10 mV), the inward proton current shown in Fig. 7 A is no longer constant, but slowly decays. This decay could arise from gating charge immobilization due to the onset of slow inactivation during the depolarizing pulse. Alternatively, since HB recording solutions were used, the decay could be due to an accumulation of HEPES buffer at the internal membrane during the depolarizing pulse and this could obstruct the proton pathway, alter the local pH around the histidine, or shift the Q-V curve.

The proton currents appear in the voltage range where gating charge displacement is most steeply voltage-dependent (Fig. 7, Rel. Q are the numbers to the right of each current trace). This is the range where transitions between hyperpolarized- and depolarized-

favored states occur very frequently. Consequently, the translocation of the histidine, which is coupled to each transition of the voltage sensor, generates a sustained proton current down the proton electrochemical gradient. Conversely, at extremely hyperpolarized or depolarized potentials, the sensor remains in one state most of the time and, therefore, the proton current approaches zero at extreme potentials. The amount of proton current observed in the OFF-gating currents is negligible and constant since all were elicited by the return to −110 mV (Fig. 7).

Proton transport due to the translocation of histidine in the R368H channel requires protonation of the 368H residue on the acidic side of the membrane and deprotonation on the basic side. This change in histidine charge, which is coupled to gating, will cause a difference in the gating charge displaced in the outwardly moving ON-gating current (Q_{on}) relative to the charge that returns in the OFF-gating current (Q_{off}). Indeed, at very depolarized potentials where both Q_{on} and Q_{off} can be measured with minimal contamination by the proton transport current, the gating charge asymmetry imposed by a pH gradient is evident (Fig. 7). In Fig. 8, 50-mV pulse evoked gating currents, recorded in three different pH_os and approximately the same pH_i are superimposed and displayed along with the integrated charge displaced by the currents. The OFF-gating currents and charge were titrated by changes in pH_o, indicating that external histidine exposure occurs in the depolarized state. The ON-gating current and charge remain constant, regardless of the 368H charge returning from the depolarized state. Therefore, the histidine is exposed to the unchanged internal solution in the hyperpolarized state where it equilibrates to the constant charge that is displaced in the ON-gating current.

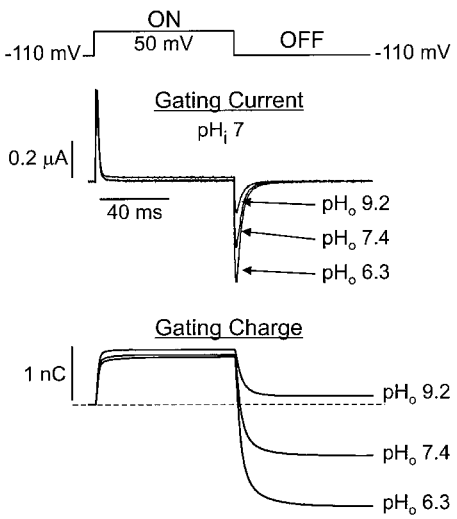

FIGURE 8. Titration of gating charge displacement in the R368H channel. The gating currents in response to a 50-mV test pulse, were recorded in three pH gradients from the same oocyte described in Fig. 7. The current records are shown here superimposed along with the corresponding gating charge displacement obtained by integrating the gating currents over the duration of the ON and OFF potential pulses. (Experiment D11200a)

In the pH_o 7.4 and pH_i 7 condition, one might expect the histidine charge to be almost the same on each side of the membrane and, consequently, nearly symmetric charge displacement. However, Q_{off} is much larger than Q_{on} (Fig. 8, pH_o 7.4). Since the histidine charge is determined by both its pK_a and the pH of the surrounding solution, the mismatched charge displacements indicate that the histidine pK_a is not the same on the internal and external side; the internal pK_a is less than the external pK_a.

One way to estimate the histidine pK_a is to examine the behavior of the proton transport current in more detail. Recall that the ON-gating current of the R368H channel is a superposition of a transient and constant current; the transient component arises from gating charge displacement (Q_{on}), and the constant component is the proton current (I_H) transported by the histidine. Therefore, the proton current amplitude at each potential can be obtained from the ON-gating currents at long durations, when the transient component has decayed to zero (Fig. 7, I_H arrow). Fig. 9 A shows the voltage dependence of R368H channel proton transport in five different pH gradients. Each pH gradient establishes a Nernst proton equilibrium potential, E_{H+}. The most obvious observation is that the I-V curve of proton transport in each pH gradient is bell-shaped or slightly biphasic. Although the direction of I_H in each pH gradient is determined by E_{H+}, conductance of protons through an open pore would have a linear, rather than bell-shaped I-V relationship. It is the shape of the proton current I-V that reveals it to be a transport current coupled to gating charge displacement, Q. For each of the five proton transport I-V curves shown in Fig. 9 A, the associated Q-V curves are shown in Fig. 9 B. Proton transport in each pH gradient appears only in a limited voltage region, approximately where the Q-V curves are not saturated. In this region, the voltage sensor makes relatively frequent transitions between states so that transport is driven both by the proton electrochemical gradient and by transitions of the voltage sensor. In each case, proton transport peaks around −30 to −50 mV (Fig. 9 A), near the potential of half-maximal charge displacement and most frequent voltage sensor transitions. The voltage dependence of proton transport resembles that of gating capacitance, C_g ($\Delta Q/\Delta V$). As expected, the proton current amplitude grows with the steepness of its associated Q-V and goes to zero both at E_{H+} and at the asymptotes of the Q-V, where there is very little change in Q with V.

To estimate pK_i, pK_o, and the location of 368H in the transmembrane electric field, the proton transport

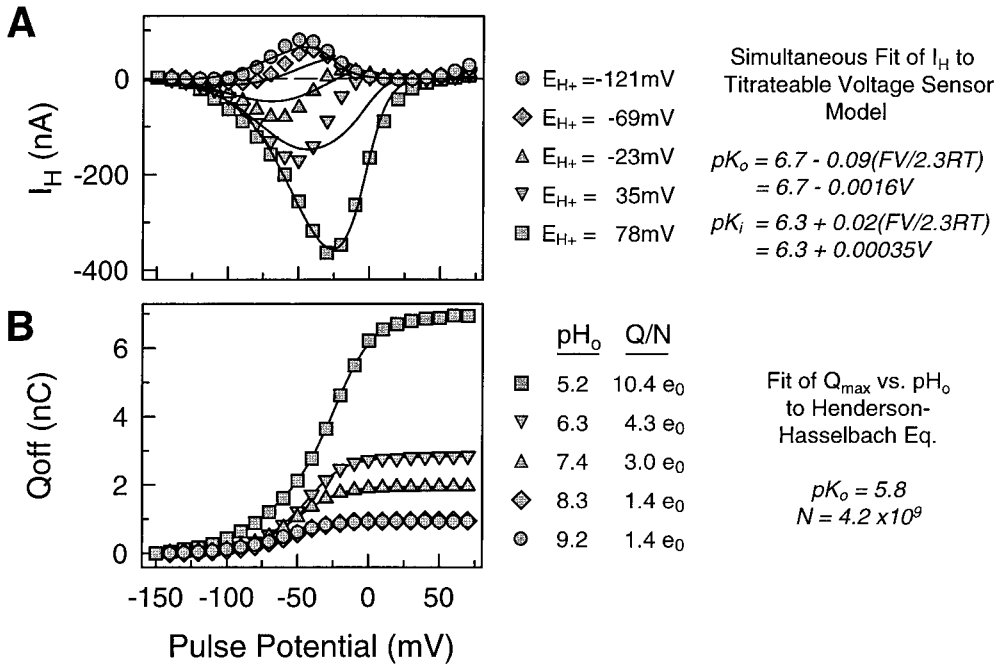

FIGURE 9. Voltage dependence of proton transport and gating charge displacement in the R368H channel. A family of pulse-evoked R368H channel gating currents and pH_i were simultaneously measured in five different pH gradients across the membrane, as described and shown for three of the gradients in Fig. 7. pH gradients were established using HB recording solutions by leaving the internal solution constant and varying pH_o: pH_o/pH_i 5.2/6.6 (■), pH_o/pH_i 6.3/6.9 (▼), pH_o/pH_i 7.4/7.0 (▲), pH_o/pH_i 8.3/7.1 (◆), and pH_o/pH_i 9.2/7.1 (●). (A) Voltage dependence of steady-state proton current amplitudes in five pH gradients (proton transport I-V curves). The Nernst equilibrium potential established by each pH gradient, E_{H+}, is also displayed. All five proton current I-V curves were simultaneously fit to an expression for proton current values predicted from a titrateable voltage sensor model (see THEORY, second term of Eq. 1) with voltage-dependent pK_as (Eq. 2). The best fit values for pK_o and pK_i are shown in two forms: first, $pK(V) = pK(0) \pm \delta(FV/2.3RT)$ to highlight δ, the fraction of the electric field sensed, followed by $pK(V)$ at room temperature to highlight the slope of the voltage dependence, where V is in units of millivolts. Other parameters of the fit are: N = 1.82e10, $z = 3.09$, $z_J = 0.061$, $\delta_{\alpha 1} = 0.012$, $\delta_{\alpha 2} = 0.376$, $\alpha_1(0) = 8464/s$, $\alpha_2(0) = 67215/s$, and $\beta_1(0) = 4775/s$. (B) Corresponding Q-V curves for the OFF-gating currents in five pH gradients. Total gating charge per channel (Q/N) was estimated by fitting Q_{max} versus pH_o to the Henderson-Hasselbach equation ($Q/N = Q_{min} + \{(Q_{max} - Q_{min})/[1 + \exp[2.3(pH_o - pK_o)]]\}$). The fit predicted a pK_o of 5.8 and saturated at a maximum value of 8.37 nC. Assuming that the fully protonated voltage sensor displaces 12.5 e_0 per channel as the wild-type, N = 8.37 nC/12.5 e_0 = 4.2e9. (Experiment D11200a)

data was fit to a model of a titrateable voltage sensor (Starace et al., 1997). The only modification to the model was the incorporation of voltage-dependent pK_as (see THEORY, Eq. 2) to accommodate the possibility that 368H is situated in a confined aqueous environment into which the transmembrane field extends. The field would alter the local pH around the histidine by affecting the access of protons to their binding site. Model-derived expressions for the proton current were simultaneously fit to all five proton transport I-V curves. The best simultaneous fit, shown in Fig. 9 A (lines), predicts that pK_i is less than pK_o, which is consistent with the charge asymmetry data (Fig. 8): at 0 mV, pK_o = 6.7 and pK_i = 6.3. The estimated voltage-dependent term in pK_o (Fig. 9 A) suggests that a proton crosses ~10% of the transmembrane field when it travels from the extracellular solution to the external histidine binding site. The estimated voltage-dependent term in pK_i, on the other hand, is only ~2%, which suggests that the internally exposed histidine binding site is not in the electric field.

Another way to estimate the pK_o of residue 368H is to examine the titration of Q_{off} with external protons since the histidine gets exposed and equilibrated to the external solution before repolarization elicits Q_{off} (Fig. 9 B). The modulation of maximum Q_{off} by pH_o was fit to a two-state model (Henderson-Hasselbach equation) that simply describes the titration of a protonatable group. The number of channels (N) was estimated from the saturating value of the fit, which is the maximum Q_{off} of N fully protonated voltage sensors. We assigned this saturating value to 12.5N based on the assumption that each fully protonated sensor displaces 12.5 e_0, like the wild type (Schoppa et al., 1992). The value of N obtained from the fit was used to calculate maximum Q/N values in other pH_os (Fig. 9 B). In pH_o 9.2 (circles), Q/N was estimated to be 1.4 e_0, a reduction of ~11 e_0 per channel, rather than 4 e_0 per channel expected from a reduction of one full charge in each subunit. The modulation of Q_{off} by pH_o fit the two-state model with a pK_o of 5.8, which is indicative of histidine titration. This estimate of pK_o was made at a potential that saturates Q_{off} and, therefore, divulges nothing about the possibility of a voltage-dependent pK_o. However, evaluation of Q/N versus pH_o at other potentials to infer the voltage dependence of pK_o would not be reliable since Q measures the displacement of the entire voltage sensor, not just the 368H res-

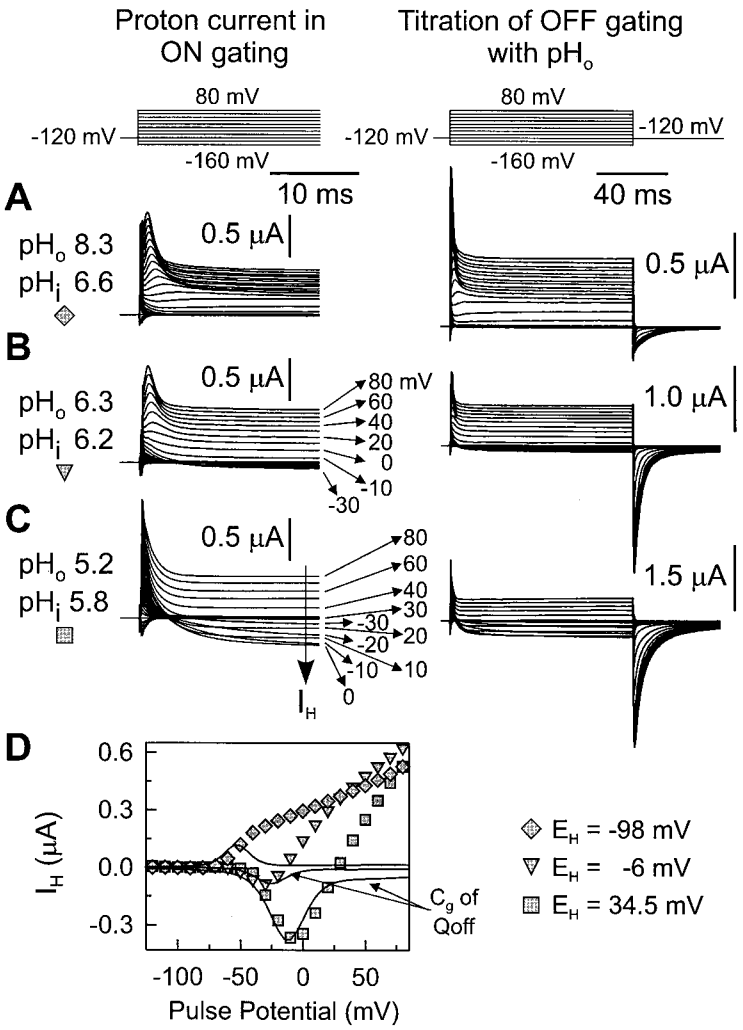

FIGURE 10. Gating currents of the R371H channel. Using the cut-open oocyte voltage clamp with a H^+ sensitive electrode, R371H channel gating currents and pH_i were simultaneously measured in three pH gradients: pH_o/pH_i 8.3/6.6 (A), pH_o/pH_i 6.3/6.2 (B), and pH_o/pH_i 5.2/5.8 (C). The gradients were established with HB recording solutions; the external solution was varied while the internal pH 5 solution was left unchanged. All gating currents were recorded from the same membrane area. The gating currents in each pH_o/pH_i group (shown superimposed in A–C) were elicited by the pulse protocol series shown at the top. The left panel of A–C is an enlargement of the ON-gating currents shown fully in the right panel. Linear leak current was subtracted from each current trace off-line as described in MATERIALS AND METHODS (*Data Analysis of I-V Curves*). (D) Voltage dependence of steady-state proton current amplitudes (proton current I-V curves) measured in three pH gradients: pH_o/pH_i 8.3/6.6 (◆), pH_o/pH_i 6.3/6.2 (▼), and pH_o/pH_i 5.2/5.8 (■). I_H was determined by taking the isochronal, steady-state amplitudes of the ON-gating currents shown in A–C. The linear leak component has already been subtracted out as described in MATERIALS AND METHODS. The Q_{off}-V curve associated with each I-V curve was used to generate the voltage dependence of the gating capacitance, C_g. Each C_g-V curve (lines) was scaled to its associated I-V curve. (Experiment D11210b)

idue. Indeed, the reduction of Q/N by 11 e_0 upon histidine deprotonation is far more than one charge per subunit because, in pH_o 9.2, the Q-V reflects not only the loss of charge on the histidine residue, but also the altered electric field and motion of the remaining voltage sensing residues.

R371H Channel. The gating currents of the R371H channel are also accompanied by bulk pH-sensitive currents, indicating translocation of the histidine at position 371 from the internal to external solution during gating (Fig. 10). However, the behavior of the R371H proton currents is notably different from the straightforward proton transport of the R365H channel (Starace et al., 1997) and the R368H channel described above. One of the most striking features of the R371H channel gating currents is that there are pH-dependent currents at very depolarized potentials even though gating charge displacement has saturated. At potentials of saturated charge displacement, the voltage sensor remains in a highly favored state most of the time with virtually no transitions to other states. Consequently, there are no accompanying histidine transitions to transport protons. We will see below that the gating currents of the R371H channel seem to be a composite of three rather than two currents: a transient charge displacement current, a proton transport current, and a novel proton current.

Fig. 10 shows pulse-evoked gating current records from R371H channels in three different pH gradients. In each gradient, the ON-gating currents are composed of the transient component produced by gating charge displacement and a steady component. I-V curves of the steady currents (Fig. 10 D) indicate that they are carried by protons since the direction of current flow in each pH gradient is determined by the Nernst proton equilibrium potential, E_{H+}. Moreover, charge displaced in the OFF-gating currents is modulated by pH_o (Fig. 10, A–C, right), indicating that once depolarized to the test pulse potential, 371H gets exposed and equilibrated to the external solution before repolarization elicits Q_{off}. The presence of proton currents in the R371H channel along with the ability to titrate the histidine during gating reveal that residue 371 traverses the membrane with each voltage sensor stroke.

The proton currents of the R371H channel do not have the bell-shaped voltage dependence expected of a transport current coupled to voltage sensor transitions. In Fig. 10 D, the proton current I-V curve in each pH gradient is displayed along with its associated C_g-V curve ($C_g = dQ/dV$). The peak of the C_g-V curve marks the voltage range of most frequent voltage sensor transitions. Each of the proton current I-V curves has a bell-shaped component that follows the corresponding C_g-V curve. In other words, the R371H channel gating currents display properties indicative of proton transport by the histidine; there is a component driven by the pH gradient and coupled to voltage sensor transitions between hyperpolarized-favored and depolarized-favored states. However, there is another component in the R371H channel gating currents: an outward current at depolarized potentials whose amplitude increases linearly with the membrane potential, more like a pore current than a transport current. This ohmic component arises after the associated gating charge displacement has saturated and C_g is negligible (Fig. 10, lines). Therefore, it is not coupled to transitions of the voltage sensor, as is the proton transport current.

It is important to recall that a nonspecific, pH-independent, linear leak current has already been subtracted from all of the current records shown. The ON-currents displayed are specific to expression of the R371H channel. They are much larger and more nonlinear than background leak currents in uninjected oocytes. Typical R371H channel expression results in at least 10^{10} channels in the recording area of the cut-open voltage clamp. The average nonlinear component of the steady-state ON-gating current evoked by a 60-mV pulse is 300 ± 36 nA (SEM) per 10^{10} R371H channels (n = 11 oocytes). In uninjected oocytes, the nonlinear component at 60 mV is 46.2 ± 23 nA (SEM; n = 7 oocytes). This is a 6.5-fold increase in nonlinear current caused by average expression of the R371H channel. The linear leak component (subtracted out from the displayed data), on the other hand, increases only 1.4-fold on expression of the R371H channel regardless of the expression level. It is very unlikely that the proton currents we observe with R371H channel expression are nonspecific currents arising from some channel native to the oocyte. It is also unlikely that the proton currents are leaking through the R371H channel K^+ pore since none of the other histidine mutants display this property.

The I-V relationship of R371H channel steady-state ON-gating currents can be interpreted in several ways. One of these is that there is no proton transport component at all, rather, the entire I-V, including the inward part of the current, is one of proton conductance through a pore formed by the histidine at position 371 (Fig. 2 D). Since the pore is not open at hyperpolarized potentials (Fig. 10 D), this interpretation requires that it be gated open by depolarization of the voltage sensor. Depolarization could drive the histidine to a position accessible to both the internal and external solutions, thereby creating a proton pathway.

Another interpretation of the behavior of the R371H channel proton currents is that, at position 371, the histidine can both transport protons and form a proton-specific pore. This interpretation implies that the proton current I-V curve has a bell-shaped component due to voltage sensor–coupled proton transport and an ohmic component that arises at depolarized potentials as the voltage sensor drives 371H to a position that bridges an internal and external space or crevice.

Both interpretations were incorporated into a simple model of a titrateable voltage sensor that not only transports protons during gating, but also forms a proton pore at depolarized potentials (Fig. 1 B). The pore model was constructed by modifying our existing model, which describes proton transport by a histidine-tagged voltage sensor (Starace et al., 1997). The details of the modified model are described in THEORY. Fig. 11 shows the result of fitting the R371H channel proton current data (symbols) to the pore model (lines). The steady-state proton current (I_H) predicted by the model is the sum of a proton transport current (I_T) and a current through a pore (I_P) formed by a single proton binding site. Considering the simplicity of the model, it mimics the proton currents of the R371H channel quite well over a large range of pH gradients (Fig. 11). The best simultaneous fit predicts significant voltage-dependent terms in all of the pK_a's, suggesting that accessible histidine sites are within the transmembrane electric field (Fig. 11). The voltage-dependent term in pK_i suggests that, in the hyperpolarized state, a proton from the internal bulk solution crosses ~37% of the field to reach the internally accessible 371H binding site. The voltage-dependent term in pK_{iP} suggests that when depolarization drives 371H to a pore-forming state, the internally accessible proton binding site moves deeper in the field, so that an internal proton crosses ~93% of the field to reach it. Finally, the voltage-dependent term in pK_o suggests that, in the depolarized state, a proton from the external solution crosses ~46% of the field to reach the externally accessible 371H site. Although, the model is far too simple to be quantitative, perhaps the interesting qualitative features of the fit present legitimate predictions.

Neither the model nor our data can discriminate between whether the R371H channel proton currents are composed purely of conductive currents or are a composite of both transport and pore currents. Although the fit shown in Fig. 11 predicts that there is a significant transport component to the R371H proton currents (I_T), fits that predict a purely conductive current

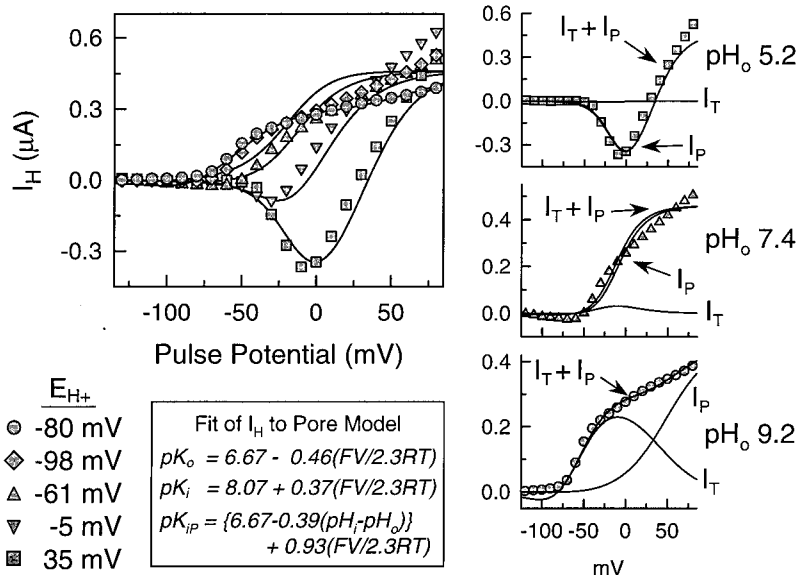

FIGURE 11. Proton transport and conduction by the R371H channel voltage sensor. I-V plots of the steady-state proton currents, I_H, measured in five different pH gradients: pH_o/pH_i 9.2/7.8 (●), pH_o/pH_i 8.3/6.6 (◆), pH_o/pH_i 7.4/6.34 (▲), pH_o/pH_i 6.3/6.2 (▼), and pH_o/pH_i 5.2/5.8 (■). The Nernst equilibrium potential established by each pH gradient, E_{H+}, is also displayed. Gating currents and pH_i were measured simultaneously as described and shown for three of the gradients in Fig. 10. All five proton current I-V curves were simultaneously fit to an expression for proton current values (see THEORY, Eq. 6) predicted from a model of a titrateable voltage sensor that forms a proton pore upon depolarization. The proton current predicted by the model is the sum of a proton transport current, I_T, and a proton pore current, I_P. The parameters of the best fit to the model (shown as lines) are: $pK_o(0)$ = 6.67, $pK_i(0)$ = 8.07, δ_o = 0.460, δ_i = 0.373, δ_{ip} = 0.934, γ_o = 93.5/s, $\varepsilon_o(0)$ = 4.33e8/(M s), γ_{ip} = 138/s, N = 3.08e10, z = 1.14, z_1 = 0.844, $\delta_{\alpha 1}$ = 0.139, $\delta_{\alpha 2}$ = 0.879, $\alpha_1(0)$ = 7247/s, $\alpha_2(0)$ = 818/s, and $\beta_1(0)$ = 2,369/s. (Experiment D11210b)

are almost as good. The model can accommodate both possibilities very crudely; parameters can be chosen that favor the conduction loop so heavily that the transport component becomes negligible. The *Shaker* K^+ channel requires a model with many more states to account for all details of the gating currents quantitatively (Bezanilla et al., 1994), so it is not surprising that our simple model is not an ideal fit to the data. Since the proton current data cannot resolve gating transitions between the resting and active states, nothing would be gained in the construction of more sophisticated models that, for example, allow pore formation from only a subset of depolarized states. Moreover, the fitted pK_a's are quite high, implying that the deprotonation rates are comparable to the gating transition rates. In this case, the assumption used in the model that there is a fast equilibrium between protonated and unprotonated states is not entirely accurate.

Regardless of the interpretation of the mechanistic details, it is clear that the gating currents of the R371H channel are dependent on the pH gradient and contain a pH-dependent transmembrane current. Therefore, the voltage sensing residue at position 371 passes from internal to external exposure during gating. Moreover, the fit of such a simple proton pore model to the data makes it is quite reasonable that residue 371H forms a proton pore in some depolarized conformations occupied by the voltage sensor.

E283Q /R371H Channel. There is evidence for the existence of charged networks between acidic residues in the S2 and S3 transmembrane segments and some of the basic residues in S4 (Tiwari-Woodruff et al., 1997, 2000). These networks presumably stabilize charges buried in the membrane by pairing them with opposite charges and may contribute to shaping the transmembrane electric field. One such network contains three participants: R368 and R371 in S4 and E283 in S2. Interaction between these residues has been demonstrated by the necessity to pair neutralization of residue E283 with neutralization of either R368 or R371 to obtain functional channels (Tiwari-Woodruff et al., 1997). Neutralization of the S2 residue (E283) in the R368H and R371H channels provides an effective way to examine residue 283's effect on the accessibility of residues 368H and 371H in both charged and uncharged states. It may also give us some insight into the nature of the proton currents carried by 371H.

Addition of the neutralizing mutation, E283Q, to the R371H channel slowed the gating current kinetics by ~10-fold (Fig. 12 A). Passage of residue 371 from internal to external exposure during gating, however, still took place. In symmetric pH 9.2 solutions, the Q-V curves for the ON- and OFF-gating currents (Fig. 12 B, circles) roughly superimpose, indicating that the 371H charge is almost the same in the initial hyperpolarized state and the pulsed depolarized state. After decreasing pH_o to 5 and thereby imposing an inward proton gradient across the membrane, Q_{off} increased (Fig. 12 B, filled squares), indicating that once depolarized, 371H gets exposed and equilibrated to the external solution before repolarization elicits Q_{off}. Q_{on} was unaffected by the change in pH_o (Fig. 12 B, open squares). Regardless of the OFF charge returning to the hyperpolarized state, 371H gets exposed and equilibrated to the unchanging internal solution before depolarization elicits Q_{on}. The asymmetry of charge displacement created by

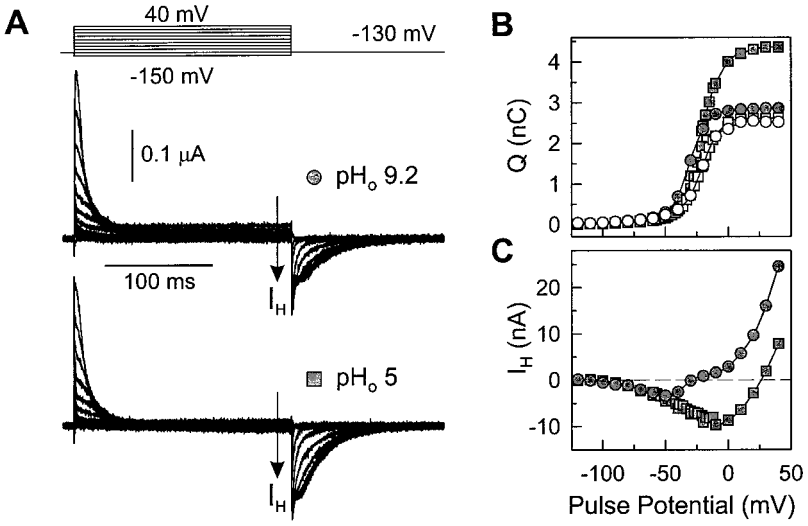

FIGURE 12. Gating currents of the E283Q/R371H channel. (A) Using the cut-open oocyte voltage clamp, E283Q/R371H channel gating currents were measured in symmetric NMDG-MS solutions with internal pH 9.2, and either pH_o 9.2 (top currents) or pH_o 5 (bottom currents). All gating currents were recorded from the same membrane area. The gating currents in each pH_o group (shown superimposed) were elicited by the pulse protocol series shown at the top. (B) Q-V curves for the ON- (open symbols) and OFF-gating currents (closed symbols) displayed in A (pH_o 9.2, circles; pH_o 5, squares). (C) The voltage dependence of steady-state ON-gating currents shown in A (circles, pH_o 9.2; squares, pH_o 5). The linear leak component has already been subtracted out, as described in MATERIALS AND METHODS (*Data Analysis of I-V Curves*). (Experiment D11037a)

a pH gradient demonstrates that even when E283 is neutralized, the histidine at position 371 passes from internal to external accessibility with each voltage sensor transition from the hyperpolarized to depolarized state.

Since E283Q/R371H channel charge displacement is asymmetric in a pH gradient, a proton current should accompany each voltage sensor stroke. However, no obvious steady-state proton current (I_H) developed in the ON-gating currents (Fig. 12 A, bottom). Only in the I-V curves of the steady-state ON-gating currents (Fig. 12 C) can one discern a small pH gradient–dependent current, reminiscent of the R371H channel proton currents. In an inward proton gradient, a very small inward current developed (Fig. 12 C, squares) in the voltage region where associated gating charge transitions were most frequent (Fig. 12 B, squares, the steepest part of the Q-V). At very depolarized potentials, an outward ohmic component arises. The properties of the steady-state ON-gating currents of the E283Q/R371H channel resemble those of the R371H channel in many respects except one: the sizes of the proton currents are dramatically reduced.

The steady-state ON-gating currents from the E283Q/R371H channel are barely above the background, making it difficult to attribute them to something as specific as proton transport and/or conduction by the histidine at position 371. However, as discussed above, the voltage dependence of the steady-state currents (Fig. 12 C) is pH-dependent and is correlated to the voltage dependence of gating charge transitions (Fig. 12 B). In fact, when the Q-V curve is shifted along the voltage axis by measuring Q starting from and holding at depolarized rather than hyperpolarized potentials, there is a corresponding shift of the associated steady-state I-V curve (data not shown). These features are highly suggestive of a proton current coupled to voltage sensor transitions.

The slow kinetics of the E283Q/R371H channel gating currents indicate slow voltage sensor transitions. The small size of the steady-state currents measured is consistent with proton transport by 371H since the transport rate expected from a channel with such slow gating currents would be correspondingly slow. Alternatively, the reduction of proton current amplitudes through a pore formed by 371H could be due to the disruption of proton selectivity by E283 neutralization. This could be accomplished by alteration of the 371H pK_a. Since positions 371 and 283 interact in depolarized states (Tiwari-Woodruff et al., 2000), neutralization of E283 could very likely perturb the 371H pK_a while in a pore-forming state. If, in the depolarized state, E283 decreases the local external pH around 371H relative to the bulk, then neutralization of E283 would effectively lower the external pK_a of the proton pore. If external proton access to the 371H pore is through a narrow, nonisopotential cavity, then E283 neutralization may alter the electric field drop through the cavity, and thereby alter the effective external pK_a of the pore. These are just a couple of the many ways that E283 neutralization could affect the 371H pK_a and cause a reduction of proton current through a pore formed by 371H. The reduction of E283Q/R371H channel proton current amplitudes is consistent with both transport and pore formation by 371H. Although E283Q neutralization makes no progress in determining the composition of R371H proton currents, it does suggest some interesting ways of designing effective proton pores.

There is evidence that residue R368 in S4 also interacts with E283 (Tiwari-Woodruff et al., 1997, 2000). However, addition of the neutralizing mutation (E283Q) to the R368H channel did not alter the gating or proton transport properties of the channel at all (data not shown).

DISCUSSION

The main observation reported in this paper is that, upon histidine replacement, the second, third, and fourth charged residues of the S4 segment each fully translocate from internal exposure at hyperpolarized potentials to external exposure at depolarized potentials.

Histidine Scanning and Accessibility of Charged Residues in S4

Most of the voltage sensing residues of the *Shaker* K^+ channel are located in the S4 segment (Aggarwal and MacKinnon, 1996; Seoh et al., 1996). Histidine scanning mutagenesis of the basic residues in S4 was used to probe the local accessibility changes that accompany gating charge movement in the *Shaker* K^+ channel. By measuring the charge moved in the gating currents of histidine-replaced channels, we could monitor the accessibility of the histidine to protons in the bulk solution if the histidine is part of the voltage sensor.

Although much attention has been focused on identifying the involvement of S4 residues in gating, there is very little known about the residues located in the cytoplasmic half of the S4 segment. Charge altering mutations of residue R377 have not generated functional channels (Aggarwal and MacKinnon, 1996). Therefore, the solvent accessibility and contribution of R377 to voltage sensing is unknown. Successful expression of the channel after replacing R377 with a histidine provides the first opportunity to examine the effect of modifying this residue. The gating currents of the R377H channel were unaffected by protons in the surrounding solution, indicating that residue 377 is either completely inaccessible or it does not move in the transmembrane electric field. The latter is perhaps more likely since cysteine scanning mutagenesis of the neighboring residue, S376, has demonstrated that 376 is exposed to internal cysteine labeling reagents in the hyperpolarized state and buried in the depolarized state (Larsson et al., 1996; Yusaf et al., 1996; Baker et al., 1998). Residue 376 is the sole residue in the cytoplasmic half of S4 for which there is exposure data published previously.

The gating currents of the K374H channel were also unaffected by protons in the surrounding solution, indicating that residue 374 is either completely inaccessible or it does not participate in gating charge displacement. Although the charge contributed by K374 to the gating current has been measured directly, the role of K374 in voltage sensing is still ambiguous (Aggarwal and MacKinnon, 1996; Seoh et al., 1996; see Table II in Bezanilla, 2000). Most mutations that neutralize the amino acid at 374 hinder functional expression of the channel. Those neutralizations that maintain channel function resulted in a reduction of two voltage sensing charges per channel, thereby implicating K374 as part of the voltage sensor (Aggarwal and MacKinnon, 1996). However, the charge conserving substitution (K374R) increased the charge per channel by 2 e_0, suggesting that K374 plays a structural rather than functional role in voltage sensing. This conjecture is consistent with the results of Papazian and her colleagues who found that the loss of function after K374 neutralization could be rescued by pairing the lethal mutation with a neutralization of either E293 or D316 in the S2 or S3 segment, respectively (Papazian et al., 1995; Tiwari-Woodruff et al., 1997). When the displaced gating charge was measured in these double mutants, it was found that there was no loss of charge in the voltage sensor as a result of neutralizing K374 (Seoh et al., 1996). Together, these data suggest that K374 makes a structural contribution to voltage sensing, perhaps by shaping the transmembrane electric field. This is consistent with the inability of solvent protons to titrate K374H gating currents if residue 374 does not contribute its charge to the gating current. Moreover, it is likely that residue 374 is also totally inaccessible since any structural alteration induced by a change in its charge might affect the gating currents even if residue 374 itself does not move in the field during gating.

The histidine scanning mutagenesis studies that we have reported here and elsewhere (Starace et al., 1997, 1998; Starace and Bezanilla, 1998) have revealed that each of the three central residues of the S4 segment, R365, R368, and R371, progresses from internal to external exposure during channel gating. A traverse of three charges per subunit across the membrane with each voltage sensor stroke would account for all 12 gating charges if the entire electric field were crossed. This would be the case if the hydrophobic region traversed by the voltage sensing charges defines the boundary of the electric field. However, as we will see in the discussion ahead, it is likely that the electric field extends beyond the hydrophobic region and into narrow aqueous spaces that penetrate it. Then, translocation of charge from the internal to external solution may not cross the entire electric field. Consequently, the traverse of R365, R368, and R371 across the membrane would not necessarily account for all 12 charges required to gate the channel. Indeed, we have found that the outermost residue R362, when replaced with a histidine, is also accessible to the internal or external solution depending on the membrane potential (Starace and Bezanilla, 1999, and in preparation).

Aqueous Crevices that Line the S4 Segment

A comparison of the histidine scanning results with published cysteine scanning results suggests that access to residues 365, 368, and 371 from the solvent is, in some cases, through narrow aqueous crevices that are too restrictive for the relatively large cysteine labeling reagents.

Residue 365, when replaced with cysteine, was accessible to internal MTSET only when extremely hyperpolarized potentials were used and the reaction rate was very slow (see personal communication discussed in Baker et al., 1998). This contrasts with the efficiency of proton transport in the R365H channel (Starace et al., 1997) and suggests that residue 365 is confined to a narrow, internally faced hydrophilic crevice in the closed, hyperpolarized state of the channel. Upon depolarization, both histidine (Starace et al., 1997) and cysteine scanning mutagenesis (Larsson et al., 1996; Baker et al., 1998) have shown that residue 365 can be accessed from the external solution.

Comparison of histidine and cysteine scanning results suggests that residue 368 is also confined to a restrictive aqueous crevice, but one in contact with the external solution. When replaced by a cysteine, the modification rate of residue 368 with external MTSET was found to be exceptionally low at depolarized potentials (Baker et al., 1998). Again, the contrast between histidine and cysteine scanning studies suggests that residue 368 resides in a narrow, externally faced crevice in the open, depolarized state of the channel. In the closed state, both histidine and cysteine scanning mutagenesis (Larsson et al., 1996; Baker et al., 1998) indicate that residue 368 is exposed to the internal solution.

The results presented in this paper suggest that the local environment around residue 371 is somewhat unique. The voltage sensing residue at position 371 is right in the middle of the putative S4 segment and there is no other published data on the exposure of this residue to the surrounding solvent. The voltage sensor–coupled proton currents of the R371H channel indicate that residue 371 traverses the membrane during gating. Therefore, the external aqueous crevice that allows access to residue 368 in the depolarized state may extend down to expose residue 371 when depolarized. Similarly, the internal crevice that extends up to residue 365 in the hyperpolarized state may also expose residue 371 in the resting, closed state.

The peculiarities of the proton current behavior of the R371H channel insinuate that residue 371 indeed dwells in a highly constrained or restricted environment such as a narrow cavity. A pH-dependent ohmic current develops in the R371H channel at depolarized potentials. One way to interpret these currents that fits reasonably well to the data is that depolarization drives 371H to a position where it bridges the internal and external solution and thereby creates a proton-binding pore. This possibility suggests that in the open state of the channel, the pathways allowing internal and external solvent access either merge at 371H in a confined one-ion binding site or come close enough for proton tunneling to occur (Green, 1998). These solvent-connected pathways penetrating the hydrophobic region around the S4 must become progressively narrower and restricted to converge on a space confined enough to confer selectivity to proton passage. If narrow and restricted enough, the solvent-connected pathways themselves may contribute to proton selectivity by constraining the solvent in a proton wire arrangement. Moreover, the transmembrane electric field could partially extend into such restricted crevices so that residue 365H, 368H, and/or 371H could sense the field and initiate voltage sensor displacement even though all three residues are solvent accessible.

Formation of a proton conducting pore by residue 371H is not so far-fetched. In fact, the gating currents of the R362H channel consist entirely of large inwardly rectified ohmic currents. A detailed characterization of these currents revealed that they arise from proton conduction through a pore formed by residue 362H once driven in towards the membrane by hyperpolarized potentials (Starace and Bezanilla, 1999; Starace, D., and F. Bezanilla, manuscript in preparation). Proton pore formation upon depolarization of 371H or hyperpolarization of 362H is each consistent with a hydrophobic region bounding the S4 segment that is reduced by the penetration of aqueous crevices to a narrow span near the top of S4. It is important to keep in mind that while pore formation may occur in the histidine-replaced channels, in the normal channel the longer and bulkier arginine at position 371 (or 362) may not be able to make the speculated bridge across the isthmus between the internal and external crevices.

Recent work by Islas and Sigworth (2001) elegantly demonstrated that aqueous cavities surround the voltage sensor. They manipulated the extension of the transmembrane electric field into the surrounding solution with ionic strength and measured the subsequent effect on gating charge movement. By fitting their data with simulations that predict the field geometry for various boundary conditions, they concluded that a narrow cavity, $\sim$20 Å deep, penetrates the hydrophobic region around S4 from the internal solution, and a shallow cavity, $\sim$3 Å deep, penetrates from the external solution. Their data also suggests that the dielectric constant of the internal cavity is quite low relative to water. The conclusions of Islas and Sigworth (2001) are in agreement with ours: the hydrophobic region around the S4 segment is likely to be penetrated by a long, restricted internal crevice that extends all the way up to residue 365 and comes very close to a shallower external cavity. This geometry would focus the transmembrane electric field to the highly voltage sensitive region near the top of the S4 segment.

Interaction between Gating Charge and the Transmembrane Electric Field

The ability to titrate the gating charge of R365H, R368H and R371H channels confirms that each of

these residues contributes charge to the gating current and therefore forms part of the voltage sensor. The participation of these central basic residues in gating charge displacement was known already from measurements of the charge per channel remaining after the neutralization of R365, R368 or R371 (Aggarwal and MacKinnon, 1996; Seoh et al., 1996). What is novel here is the result that each of these residues fully translocates from inside to outside exposure during gating. Consequently, the proton transport currents in histidine-tagged voltage sensors provide an independent measurement of voltage sensor transitions and can therefore provide some constraints necessary to tease apart the contributions of charge and fraction of the electric field traversed.

Charge displacement measurements (Q) reflect the product of the charge and the fraction of the electric field it traverses; the two quantities cannot be experimentally separated with gating current experiments. Therefore, neutralization of one charge in all four subunits does not necessarily result in a reduction of 4 e_0 per channel as measured by gating charge displacement. If the missing charge traversed only a fraction of the field during gating, then the charge per channel may be reduced by less than four; if removal of the charge attenuates the movement of the remaining charges and/or alters the field sensed by them, then the charge per channel may be diminished by more than four. Indeed, such interaction between gating charge and the electric field was suggested when various voltage sensing residues were replaced by neutral residues and the charge in each of these channels was decreased by greater than 4 e_0 (Aggarwal and MacKinnon, 1996; Seoh et al., 1996). A more direct indication of this interaction is shown in this study where deprotonation of the histidine in all three channels (R365H, R368H and R371H) reduced the gating charge displacement by at least 8 e_0 per channel compared with the fully protonated form. Assuming that the fully protonated form of the histidine-tagged voltage sensor behaves as the wild type, the excess charge removed upon deprotonation may be due to an alteration of the electric field by the unprotonated form of the histidine. The concept that the charges normally dwell in aqueous crevices helps in understanding how such an alteration could take place. In terms of the crevice view, deprotonation of the histidine could interrupt the aqueous crevice and effectively extend the region of protein that the field spans. The remaining gating charges would consequently cross a smaller fraction of the field, resulting in a >4 e_0 reduction in total charge displacement.

The ability to track the actual gating charge with proton transport measurements as well as its influence on the electric field with charge displacement measurements provides a unique opportunity to examine the local electric field. However, such an analysis is not straightforward since the field probably extends some distance into the crevices lining the S4 segment. With a purely aqueous cavity, electrostatic calculations predict that as much as 10% of the membrane potential could extend out from the membrane and drop along a narrow cavity ~20 Å in length (Islas and Sigworth, 2001). In the restricted, long internal cavity proposed, one would expect an even greater drop of the field. The behavior of proton transport in some of the channels with histidine-tagged voltage sensors is consistent with an extension of the electric field into the crevices since, to best fit the data, the histidine pK_a required a voltage-dependent term describing a proton binding site within an electric field. Fitting the proton transport data and charge displacement data to simple models of a titrateable voltage sensor suggests that a significant fraction of the field extends into the internal crevice. This type of analysis has the potential to provide estimates of the field strength in the environment of each gating charge. However, more sophisticated models that incorporate both the geometry and other gating transitions would be required for accurate predictions.

A Model of Voltage Sensor Movement

The structure imposed by the hydrophilic crevices lining the S4 segment is exquisitely voltage- sensitive. It focuses the transmembrane electric field in a narrow region onto the highly charged region near the top of the S4 segment. This enables a small conformational change to accomplish the work of moving a lot of charge across the entire transmembrane field. We have proposed a model of the movement of the S4 segment based on spectroscopic data (Cha et al., 1999; Glauner et al., 1999; Bezanilla, 2000) and some of the data presented in this paper. The model is illustrated in Fig. 13 to highlight some of the pertinent features discussed here. In the closed state (left side), the first four charges of the S4 segment lie in a narrow hydrophilic crevice that exposes them to the intracellular solution. The hydrophobic region surrounding the internal crevice is represented as a hatched cloud shaped by the membrane and the hydrophobic amino acids in the S1 and S5 segments. The crevice is shown to get progressively narrower as it reaches residues 365 and 362, since these positions are accessible to protons (Starace et al., 1997; Starace and Bezanilla, 1999), but not to larger cysteine reactive reagents (Baker et al., 1998). Depolarization causes a rotation of the S4 segment (Cha et al., 1999) and movement of the first four charges to an externally facing crevice (Fig. 13, right side). For the sake of simplicity, a 180° rotation of S4 is shown in Fig. 13. Therefore, the external crevice cannot be seen; it faces the back between the S2 and S3 segments. Our model shows how a simple rotation of the S4 segment, without

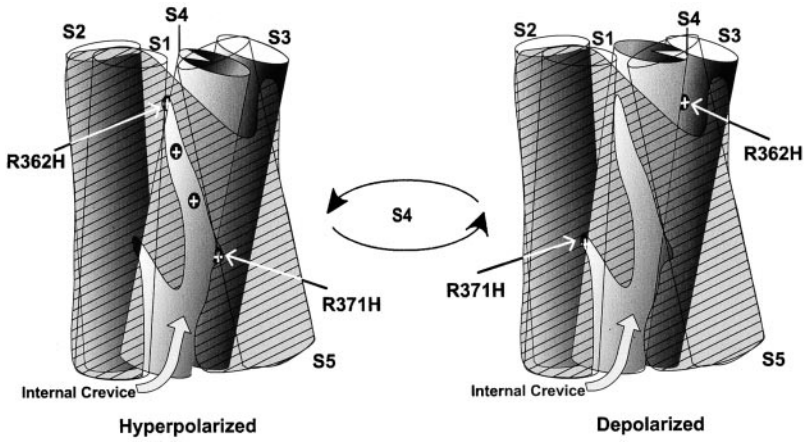

FIGURE 13. A model of voltage sensor operation. A model illustrating the movement of the *Shaker* K^+ channel S4 segment from a hyperpolarized position (left) to a depolarized position (right). Only five transmembrane segments (S1–S5) of one subunit are shown for clarity. The hydrophobic region surrounding the internal crevice is represented as a hatched cloud shaped by the membrane and the sides of S1 and S5 facing each other. Depolarization causes a rotation of the S4 segment and movement of the first four S4 charges from the internal crevice to an externally facing crevice. The external crevice cannot be seen; it faces the back between the S2 and S3 segments.

translation, can accomplish a large charge translocation with a relatively small movement.

The model shown in Fig. 13 also conveys the potential for proton conduction by residues 362H and 371H. In the hyperpolarized state, 362H is shown at the apex of the internal crevice. At this position, the hydrophobic region is so narrow that a histidine could bridge the gap and create a proton pore (Starace and Bezanilla, 1999; Starace, D., and F. Bezanilla, manuscript in preparation). Depolarization moves 362H away from the membrane and disrupts the pore. Our data suggest that extreme depolarizations drive 371H to a position where it can also bridge the internal and external crevices and thereby create a proton-conducting pore. This is represented in Fig. 13 by bringing the internal crevice close to the external crevice in the vicinity of residue 371H when in the depolarized position.

The S4 model indicates that all of the S4 voltage sensing charges are exposed to the bulk solution: through the internal crevice in the hyperpolarized state and through the external crevice in the depolarized state. For these charges to sense the membrane potential, the field must extend into the crevices or/and other voltage sensing elements must initiate movement of the S4 segment. In fact, there is evidence that a substantial portion of the field extends into the internal crevice, as discussed above. The location of residues 362, 365, 368, and 371 in a nonisopotential crevice also solves the problem of how four charges in each channel subunit could cross the membrane and transfer only 12 to 13 e_0 across the transmembrane field (Schoppa et al., 1992; Aggarwal and MacKinnon, 1996; Noceti et al., 1996; Seoh et al., 1996), rather than 16 e_0. With the field dropping along the internal crevice, although four charges may traverse the membrane, each may cross a different fraction of the total field and thereby contribute less than 1 e_0 per subunit. At this point it is not possible to predict the contribution of each of the gating charges because we do not have reliable estimates of the local field strength. The simplest assumption is that the deeper residues (i.e., 365 in the internal crevice) traverse a smaller fraction of the field than the residues closer to the entrance of the crevice (i.e., residue 371 in the internal crevice). However, this assumption could fail if there were residues near the entrance of the crevice deeply embedded in the side chains of neighboring segments. For example, let us assume that the voltage dependence of the internal pK_a of residue 371H (pK_i, Fig. 11) were an accurate estimate of the fraction of the field sensed by 371H in the closed state. Then upon depolarization, residue 371H would only cross the remaining 63% of the field at most and contribute two thirds of a charge to the total gating current. However, the contribution of the wild-type charge (R371) is likely to be quite different from that of 371H when we consider the differences in volume and chain length between arginine and histidine.

The accessibility of each S4 gating charge to the internal solution at hyperpolarized potentials and to the external solution at depolarized potentials eliminates the necessity for stabilizing counterions in other transmembrane segments. Rather, the gating charges may be hydrated and/or surrounded by anions present in the bulk solution, which lowers their conformational energies. Therefore, a traverse of the hydrophobic part of the molecule would present a large energy barrier separating the resting from the active state of the channel, making spontaneous crossings a rare event. Application of an electric field would lower this energy barrier and increase the rate of gating charge transitions.

The Histidine-tagged Voltage Sensors: General Mechanisms of Proton Transport?

It is quite surprising that a single histidine mutation can transform the voltage sensor of a K^+ channel into an efficient voltage-dependent proton transporter or a voltage-gated proton channel. The transport or con-

duction of protons in these artificial constructs is driven both by the membrane potential and the transmembrane pH gradient. It is conceivable that the proton transport mechanisms described and modeled here could be found to occur naturally, perhaps involved in the regulation of intracellular or intraorganelle pH with the membrane potential. Recently, the first sequence of a voltage-gated H^+ channel was published (Bánfi et al., 2000). Remarkably, the third putative transmembrane domain contains a motif (**H**SAI**H**-TIA**H**) reminiscent of voltage sensor motifs in the S4 segments of K^+ channels (**R**VI**R**LV**R**VF**R**) where the permanently charged arginines have been replaced by histidines which allow the exchange of protons. Electrophysiological analysis of mutated versions of a homologue of this H^+ channel suggests that the histidines indeed contribute to voltage gating, H^+ permeation and H^+ selectivity (Henderson and Meech, 1999). Moreover, the M2 ion channel of the Influenza A virus contains a functionally critical histidine residue lining its pore. Interaction of protons with this histidine is essential for the channel's gating, H^+ selectivity and H^+ transport (Mould et al., 2000). The growing number of examples of histidine involvement in natural proton permeation leads us to the intruiging possibility that the operation of a histidine-tagged voltage sensor provides valuable insights to proton transport and conduction mechanisms, as well as to the voltage sensing mechanism in K^+ channels.

The authors would like to thank Dr. Daniel Sigg for many helpful discussions. Our thanks also go to Professor Ana Correa and all members of the Bezanilla laboratory for their support.

This work was supported by National Institutes of Health grant GM30376.

Submitted: 1 August 2000
Revised: 30 March 2001
Accepted: 2 April 2001

REFERENCES

Aggarwal, S.K., and R. MacKinnon. 1996. Contribution of the S4 Segment to Gating Charge in the *Shaker* K^+ Channel. *Neuron.* 16: 1169–1177.

Armstrong, C.M., and F. Bezanilla. 1973. Currents related to movement of the gating particles of the sodium channels. *Nature.* 242: 459–461.

Baker, O.S., H.P. Larsson, L.M. Mannuzzu, and E.Y. Isacoff. 1998. Three transmembrane conformations and sequence-dependent displacement of the S4 domain in *Shaker* K^+ channel gating. *Neuron.* 20:1283–1294.

Bánfi, B., A. Maturana, S. Jaconi, S. Arnaudeau, T. Laforge, B. Sinha, E. Ligeti, N. Demaurex, and K.-H. Krause. 2000. A mammalian H^+ channel generated through alternative splicing of the NADPH oxidase homolog NOH-1. *Science.* 287:138–142.

Bezanilla, F. 2000. The voltage sensor in voltage-dependent ion channels. *Physiol. Rev.* 80:555–592.

Bezanilla, F., E. Perozo, and E. Stefani. 1994. Gating of *Shaker* K^+ channels: II. The components of gating currents and a model of channel activation. *Biophys. J.* 66:1011–1021.

Cha, A., G.E. Snyder, P.R. Selvin, and F. Bezanilla. 1999. Atomic scale movement of the voltage-sensing region in a potassium channel measured via spectroscopy. *Nature.* 402:809–813.

Eigen, M., G.G. Hammes, and K. Kustin. 1960. Fast reactions of imidazole studied with relaxation spectrometry. *J. Am. Chem. Soc.* 82: 3482–3483.

Glauner, K.S., L.M. Mannuzzu, C.S. Gandhi, and E.Y. Isacoff. 1999. Spectroscopic mapping of voltage sensor movement in the *Shaker* potassium channel. *Nature.* 402:813–817.

Green, M.E. 1998. A resonance model gives the response to membrane potential for an ion channel. *J. Theor. Biol.* 193:475–483.

Hamill, O.P., A. Marty, E. Neher, B. Sakmann, and F.J. Sigworth. 1981. Improved patch-clamp techniques for high-resolution current recording from cells and cell-free membrane patches. *Pflügers Arch.* 391:85–100.

Henderson, L.M., and R.W. Meech. 1999. Evidence that the product of the human X-linked CGD gene, gp91-*phox*, is a voltage-gated H^+ pathway. *J. Gen. Physiol.* 114:771–786.

Hille, B. 1992. Ionic Channels of Excitable Membranes. 2nd ed. Sinauer Associates, Inc., Sunderland, MA. 607 pp.

Ho, S.N., H.D. Hunt, R.M. Horton, J.K. Pullen, and L.R. Pease. 1989. Site-directed mutagenesis by overlap extension using the polymerase chain reaction. *Gene.* 77:51–59.

Hodgkin, A.L., and A.F. Huxley. 1952. A quantitative description of membrane current and its application to conduction and excitation in nerve. *J. Physiol.* 117:500–544.

Hoshi, T., W.N. Zagotta, and R.W. Aldrich. 1990. Biophysical and molecular mechanisms of *Shaker* potassium channel inactivation. *Science.* 250:533–538.

Islas, L.D., and F.J Sigworth. 2001. Electrostatics and the gating pore of *Shaker* potassium channels. *J. Gen. Physiol.* 117:69–90.

Kasianowicz, J.J., and S.M. Bezrukov. 1995. Protonation dynamics of the α-toxin ion channel from spectral analysis of pH-dependent current fluctuations. *Biophys. J.* 69:94–105.

Keynes, R.D., and E. Rojas. 1974. Kinetics and steady-state properties of the charges system controlling sodium conductance in the squid giant axon. *J. Physiol.* 239:393–434.

Kozak, M. 1991. Structural features in eukaryotic mRNAs that modulate the initiation of translation. *J. Biol. Chem.* 266:19867–19870.

Larsson, H.P., O.S. Baker, D.S. Dhillon, and E.Y. Isacoff. 1996. Transmembrane movement of the *Shaker* K^+ channel S4. *Neuron.* 16:387–397.

MacKinnon, R. 1991. Determination of the subunit stoichiometry of a voltage-activated potassium channel. *Nature.* 350:232–235.

Mould, J.A., J.E. Drury, S.M. Frings, U.B. Kaupp, A. Pekosz, R.A. Lamb, and L.H. Pinto. 2000. Permeation and activation of the M_2 ion channel of influenza A virus. *J. Biol. Chem.* 275:31038–31050.

Noceti, F., P. Baldelli, X. Wei, N. Qin, L. Toro, L. Birnbaumer, and E. Stefani. 1996. Effective gating charges per channel in voltage-dependent K^+ and Ca^{2+} channels. *J. Gen. Physiol.* 108:143–155.

Papazian, D.L., X.M. Shao, S.-A. Seoh, A.F. Mock, Y. Huang, and H. Wainstock. 1995. Electrostatic interactions of S4 voltage sensor in *Shaker* K^+ channel. *Neuron.* 14:1293–1301.

Perozo, E., R. MacKinnon, F. Bezanilla, and E. Stefani. 1993. Gating currents from a nonconducting mutant reveal open-closed conformations in *Shaker* K^+ channels. *Neuron.* 11:353–358.

Root, M.J., and R. MacKinnon. 1994. Two identical noninteracting sites in an ion channel revealed by proton transfer. *Science.* 265: 1852–1856.

Schoppa, N.E., K. McCormack, M.A. Tanouye, and F.J. Sigworth. 1992. The size of gating charge in wild-type and mutant *Shaker* potassium channels. *Science.* 255:1712–1715.

Schwarz, T.L., B.L. Tempel, D.M. Papazian, Y.N. Jan, and L.Y. Jan. 1988. Multiple potassium-channel components are produced by

alternative splicing at the *Shaker* locus in *Drosophila*. *Nature*. 331: 137–142.

Seoh, S.-A., D. Sigg, D.M. Papazian, and F. Bezanilla. 1996. Voltage-sensing Residues in the S2 and S4 segments of the *Shaker* K^+ channel. *Neuron*. 16:1159–1167.

Sigg, D., F. Bezanilla, and E. Stefani. 1994. Slowing of deactivation kinetics in *Shaker* B as seen in macropatch recordings of gating and ionic currents. *Biophys. J.* 66:A439. (Abstr.)

Starace, D., and F. Bezanilla. 1998. Accessibility studies of *Shaker* K channel S4 residues by histidine scanning mutagenesis. *Biophys. J.* 74:A254. (Abstr.)

Starace, D., and F. Bezanilla. 1999. Histidine at position 362 causes inwardly rectifying H^+ conduction in the *Shaker* K channel. *Biophys. J.* 76:A266. (Abstr.)

Starace, D.M., E. Stefani, and F. Bezanilla. 1997. Voltage-dependent proton transport by the voltage sensor of the *Shaker* K^+ channel. *Neuron*. 19:1319–1327.

Starace, D., E. Stefani, and F. Bezanilla. 1998. Histidine scanning mutagenesis indicates full translocation of two charges of the *Shaker* K channel voltage sensor. *Biophys. J.* 74:A215. (Abstr.)

Stefani, E., and F. Bezanilla. 1998. Cut-open oocyte voltage-clamp technique. *Methods Enzymol.* 293:300–318.

Timpe, L.C., T.L. Schwarz, B.L. Tempel, D.M. Papazian, Y.N. Jan, and L.Y. Jan. 1988. Expression of functional potassium channels from *Shaker* cDNA in *Xenopus* oocytes. *Nature*. 331:143–145.

Tiwari-Woodruff, S.K., C.T. Schulteis, A.F. Mock, and D.M. Papazian. 1997. Electrostatic interactions between transmembrane segments mediate folding of *Shaker* K^+ channel subunits. *Biophys. J.* 72:1489–1500.

Tiwari-Woodruff, S.K., M.A. Lin, C.T. Schulteis, and D.M. Papazian. 2000. Voltage-dependent structural interactions in the *Shaker* K^+ channel. *J. Gen. Physiol.* 115:123–138.

Yang, N., A.L. George, Jr., and R. Horn. 1996. Molecular basis of charge movement in voltage-gated sodium channels. *Neuron*. 16: 113–122.

Yang, N., and R. Horn. 1995. Evidence for voltage-dependent S4 movement in sodium channels. *Neuron*. 15:213–218.

Yusaf, S.P., D. Wray, and A. Sivaprasadarao. 1996. Measurement of the movement of the S4 segment during the activation of a voltage-gated potassium channel. *Pflügers Arch.* 433:91–97.